

1 **Seasonal variations of ultrafine and sub-micron aerosols in Taipei,**  
2 **Taiwan: implications for particle formation processes in urban areas**

3  
4 **Cheung, H. C.<sup>1</sup>, Chou, C. C.-K.<sup>1,\*</sup>, Chen, M.-J.<sup>1</sup>, Huang, W.-R.<sup>1</sup>, Huang, S.-H.<sup>1</sup>,**  
5 **Tsai, C.-Y.<sup>1</sup>, Lee, C. S. L.<sup>2</sup>**

- 6 1. Research Center for Environmental Changes, Academia Sinica, Taipei 11529,  
7 Taiwan  
8 2. Institute of Occupational Medicine and Industrial Hygiene, College of Public  
9 Health, National Taiwan University, Taipei, Taiwan

10  
11 *\*Correspondence to: C. C.-K. Chou (ckchou@rcec.sinica.edu.tw)*

12  
13 **Abstract**

14 The aim of this study is to investigate the seasonal variations in the physicochemical  
15 properties of atmospheric ultrafine particles (UFPs,  $d \leq 100\text{nm}$ ) and submicron  
16 particles ( $\text{PM}_{10}$ ,  $d \leq 1\mu\text{m}$ ) in an East-Asian urban area, which are hypothesized to be  
17 affected by the interchange of summer and winter monsoons. An observation  
18 experiment was conducted at the TARO (Taipei Aerosol and Radiation Observatory),  
19 an urban aerosol station in Taipei, Taiwan, from October 2012 to August 2013. The  
20 measurements included the mass concentration and chemical composition of UFPs  
21 and  $\text{PM}_{10}$ , as well as the particle number concentration (PNC) and number size  
22 distribution (PSD) with size range of 4-736 nm. The results indicated that the mass  
23 concentration of  $\text{PM}_{10}$  was elevated during cold seasons with peak level of  $18.5 \mu\text{g m}^{-3}$   
24 in spring, whereas the highest UFPs concentration was measured in summertime with  
25 a mean of  $1.64 \mu\text{g m}^{-3}$ . Moreover, chemical analysis revealed that the UFPs and  $\text{PM}_{10}$   
26 were characterized by distinct composition; UFPs were composed mostly of organics,  
27 whereas ammonium and sulfate were the major constituents in  $\text{PM}_{10}$ . The seasonal  
28 median of total PNCs ranged from  $13.9 \times 10^3 \text{ cm}^{-3}$  in autumn to  $19.4 \times 10^3 \text{ cm}^{-3}$  in  
29 spring. The PSD information retrieved from the corresponding PNC measurements  
30 indicated that the nucleation mode PNC ( $N_{4-25}$ ) peaked at  $11.6 \times 10^3 \text{ cm}^{-3}$  in winter,  
31 whereas the Aitken mode ( $N_{25-100}$ ) and accumulation mode ( $N_{100-736}$ ) exhibited  
32 summer maxima at  $6.0 \times 10^3$  and  $3.1 \times 10^3 \text{ cm}^{-3}$ , respectively. The change in PSD  
33 during summertime was attributed to the enhancement in the photochemical  
34 production of condensable organic matter that, in turn, contributed to the growth of  
35 aerosol particles in the atmosphere. In addition, clear photochemical production of  
36 particles was observed, mostly in summer season, which were characterized by  
37 averaged particle growth and formation rates of  $4.0 \pm 1.1 \text{ nm h}^{-1}$  and  $1.4 \pm 0.8 \text{ cm}^{-3} \text{ s}^{-1}$ ,  
38 respectively. The prevalence of new particle formation (NPF) in summer was

39 suggested as a result of seasonally enhanced photochemical oxidation of SO<sub>2</sub> that  
40 contributed to the production of H<sub>2</sub>SO<sub>4</sub>, and low level of PM<sub>10</sub> ( $d \leq 10\mu\text{m}$ ) that served  
41 as the condensation sink. Regarding the sources of aerosol particles, correlation  
42 analysis upon the PNCs against NO<sub>x</sub> revealed that the local vehicular exhaust was the  
43 dominant contributor of the UFPs throughout the year. On the contrary, the Asian  
44 pollution outbreaks had significant influence in the PNC of accumulation mode  
45 particles during the seasons of winter monsoons. The results of this study implied the  
46 significance of secondary organic aerosols in the seasonal variations of UFPs and the  
47 influences of continental pollution outbreaks in the downwind areas of Asian  
48 outflows.

## 49 **1. Introduction**

50 Due to the significant impact of particulate matter on human health and climate  
51 change, it is vital to understand the formation process of atmospheric particles  
52 (Charlson et al., 1992; Donaldson et al., 1998). A number of mechanisms have been  
53 proposed by which atmospheric particles are formed, including binary nucleation,  
54 ternary nucleation and ion-induced nucleation for charged particles, under different  
55 environment conditions (Kulmala 2003; Kulmala et al., 2004, 2012). Numerous  
56 studies have been conducted in different locations to elucidate particle formation  
57 processes under various environmental settings in the free troposphere, boreal forest  
58 and coastal areas, where new particles formation processes are observed frequently  
59 (Kulmala et al., 2004, Holmes 2007). Recently, investigations were also carried out on  
60 new particle formation within urban boundary layer (e.g., Cheung et al., 2013 and  
61 references therein), where particle formation was suggested to be mainly influenced  
62 by the photo-oxidation of SO<sub>2</sub>. Furthermore, formation of particulate matter by  
63 heterogeneous reactions of gases on dust particles was reported recently (Hsu et al.,  
64 2014, Nie et al., 2014). Previous investigations have indicated that the air pollutants,  
65 both in gaseous and particulate form, associated with the continental outflows of air  
66 masses could have affected a wide region in East Asia and caused severe regional air  
67 pollution (e.g., Lin et al., 2004; Wang et al., 2003). However, the formation processes  
68 of ultrafine particles (UFPs,  $d \leq 100\text{nm}$ ) and sub-micron particles (PM<sub>1</sub>,  $d \leq 1\mu\text{m}$ )  
69 under the influences of continental outflows are not yet well understood.

70

71 In urban environment, major contributing sources of aerosol particles include  
72 vehicular exhausts (e.g., Pey et al., 2008; Pérez et al., 2010), industrial emissions  
73 (Gao et al., 2009) and new particle formation by photochemical reactions (e.g., Pey et  
74 al., 2009). Approximately 55-69% of the total particle number concentrations (PNCs)  
75 were attributed to secondary aerosols during midday in several European cities  
76 (Reche et al., 2011). In Taipei, Taiwan, a subtropical urban area, Cheung et al. (2013)  
77 observed that there was a ten-fold increase in nucleation mode particle number  
78 concentrations (N<sub>9-25</sub>, with size  $9 < d < 25\text{nm}$ ) during new particle formation events  
79 compared to that contributed by the vehicle emission. Besides the local sources, air  
80 quality of East Asian countries is also strongly affected by the transport of air  
81 pollutants from mainland China during periods of winter monsoons (Cheung et al.,  
82 2005; Lin et al., 2004; Matsumoto et al., 2003). Lin et al. (2004) reported that the  
83 mass concentration of particulate matter (PM<sub>10</sub>) due to the long-range transport  
84 associated with winter monsoons was  $85 \mu\text{g m}^{-3}$ , about 79% higher than that due to  
85 local pollution ( $\sim 47.4\mu\text{g m}^{-3}$ ) in urban Taipei. Chemical composition of fine and  
86 coarse particles was measured during a winter monsoon period at Rishiri Island, near

87 the northern tip of Japan, to study the transport of continental aerosols (Matsumoto et  
88 al., 2003). The results showed that higher levels of particle mass concentrations were  
89 associated with the outbreaks of continental polluted air masses. In addition, Cheung  
90 et al. (2005) found deterioration in visibility around the southern China during  
91 wintertime as indicated by a two-fold increase in aerosol light scattering coefficient  
92 under the influences of winter monsoons. All these studies were limited to  
93 measurements in terms of PM<sub>10</sub> or PM<sub>2.5</sub> for a particular period, and the seasonal  
94 variations of particles in either ultrafine or sub-micron range have not been well  
95 illustrated.

96

97 A 1-year aerosol characterization experiment was conducted in the urban area of  
98 Taipei, Taiwan. The aim of this study is to attain a better understanding of the  
99 seasonal variations of ultrafine and sub-micron particles and the factors affecting  
100 particle formation, particularly under the influences of Asian monsoon circulations. In  
101 this study, we analyzed number concentration and size distribution of aerosol particles,  
102 together with the mass concentration and chemical composition of UFPs and PM<sub>1</sub>  
103 measured during four seasonal campaigns (i.e. 24 Oct – 15 Nov 2012, 4 – 24 Jan, 17  
104 Mar – 11 Apr, and 1 – 14 Aug 2013). The results of this study will contribute to the  
105 management strategies of the severe air pollution over the East Asia region.

106

## 107 **2. Methodology**

### 108 **2.1 Observation site and instrumentation**

109 The measurements were conducted at the Taipei Aerosol and Radiation  
110 Observatory (TARO, 25.02 N, 121.53 E), located in the downtown area of Taipei,  
111 Taiwan, during October 2012 to August 2013. The measurements were carried out for  
112 2 – 3 weeks in each season (see **Table 1** for measurement details). The aerosol  
113 observatory locates on the top floor of the Building-B of the Department of  
114 Atmospheric Sciences, National Taiwan University (ASNTU), which is ~20 m a.g.l.  
115 (Cheung et al., 2013).

116

117 Particle number size distribution (PSD) in the range of 4 – 736 nm was measured  
118 by two scanning mobility particle sizer (SMPS) systems. One was equipped with a  
119 long-differential mobility analyzer (long-DMA, Model: TSI 3081, TSI Inc.) and a  
120 condensation particle counter (CPC) (Model: TSI 3022A, TSI Inc.) to measure the  
121 particles from 10 – 736 nm, which was named long-SMPS. Another one was equipped  
122 with a nano-DMA (Model: TSI 3085, TSI Inc.) and an ultrafine water-based CPC  
123 (UWCPC, Model: TSI 3786, TSI Inc.) to measure the particles from 4 – 110 nm,  
124 which was named nano-SMPS. The poly-disperse particles were classified into

125 selected mono-disperse particles according to their electric mobility by the DMAs.  
126 The number concentration of the mono-disperse particles was then counted by the  
127 CPCs. Ambient air was drawn into the SMPS systems from outside the building  
128 through a 0.635 cm (inner diameter) conductive tube, and a sampling duration of 5  
129 min was adopted for each PSD measurement. The SMPS systems' flow rates were  
130 checked weekly during the sampling period and the accuracy of the particle sizing of  
131 the DMAs was checked using polystyrene latex (PSL) spheres before the campaigns.  
132 Operation details are referred to Cheung et al. (2013).

133

134 Size segregated aerosol samples were collected by a pair of Micro-Orifice  
135 Uniform Deposition Impactors (MOUDI, Model: 110, MSP Corp.). Taking the  
136 advantage that the cut diameter of the 9<sup>th</sup> MOUDI impaction stage was exactly 100  
137 nm, the 10<sup>th</sup> impaction stage (cut diameter = 56 nm) of each MOUDI was removed to  
138 allow the after filter function as a collector of UFPs (Marple et al., 1991). The  
139 sampling flow rate of MOUDI sampler was 30 lpm. Besides, a pair of PM<sub>1</sub> samplers,  
140 each consisted of a standard aerosol sampler (PQ-200, BGI Inc.) and a PM<sub>1</sub> sharp cut  
141 cyclone, were deployed to collect PM<sub>1</sub> samples with 16.7 lpm sampling flow rate. For  
142 both UFPs and PM<sub>1</sub> sampling arrangements, one of the paired samplers was equipped  
143 with Teflon filters, whereas another was equipped with quartz fiber filters. The Teflon  
144 filter samples were used for gravimetric measurement. The quartz filter samples were  
145 deployed for analysis of soluble ions (Na<sup>+</sup>, NH<sub>4</sub><sup>+</sup>, K<sup>+</sup>, Ca<sup>2+</sup>, Mg<sup>2+</sup>, Cl<sup>-</sup>, NO<sub>2</sub><sup>-</sup>, NO<sub>3</sub><sup>-</sup>,  
146 SO<sub>4</sub><sup>2-</sup>) using ion chromatograph (IC), and carbonaceous components (i.e. OC and EC)  
147 in the aerosols using a DRI-2001A carbonaceous aerosol analyzer with IMPROVE-A  
148 protocol (Chow et al., 2007). Details of the in-lab analysis are as described previously  
149 (Salvador and Chou, 2014). Both the PM<sub>1</sub> and UFPs were collected with  
150 double-layered quartz filters (i.e. QBQ setup) and the artifacts due to adsorption of  
151 gaseous components were corrected as suggested by Subramanian et al. (2004). The  
152 sampling duration of each sample set (for both MOUDI and PQ-200 samplers) was  
153 from 14:00 - 12:00 LT (22 hr), and a total of 69 and 75 sets of UFPs and PM<sub>1</sub> samples  
154 were collected during the entire investigation period (sample sets collected in autumn,  
155 winter, spring and summer were 20, 15, 25, and 9 sets for UFPs, and 21, 16, 25, and  
156 13 sets for PM<sub>1</sub>, respectively).

157

158 Moreover, to assist the data interpretation, the hourly averaged mass  
159 concentration of PM<sub>10</sub>, the mixing ratio of trace gases (i.e. NO<sub>x</sub>, SO<sub>2</sub> and O<sub>3</sub>) and the  
160 meteorology parameters (i.e. wind direction/speed and UVB) from the Guting air  
161 quality station of Taiwan Environmental Protection Agency, which is about 1 km from  
162 the TARO, were analyzed in this study. The details of instrumentation setup for trace

163 gases measurement are referred to Cheung et al. (2013).

164

## 165 **2.2 Data processing and analysis**

166 The PSD of 4 – 736 nm presented in this study was combined from two sets of  
167 SMPS data, where the nano-SMPS corresponded to the size range of 4 – 49.6 nm, and  
168 the long-SMPS corresponded to the size > 49.6 nm. The diffusion loss of the particles  
169 during the sample transport in the tubing was corrected according to the algorithm  
170 proposed by Holman (1972). Particle number concentrations for different size ranges  
171 were then calculated from the SMPS measurements.

172 The 5-min PSD data were synchronized into hourly averages, and fitted by the  
173 DO-FIT model developed by Hussein et al. (2005) according to the multiple  
174 log-normal distribution algorithms. Based on the fitted PSD data, the PNCs were  
175 classified into  $4 \leq d \leq 25$  nm ( $N_{4-25}$ ),  $25 < d \leq 100$  nm ( $N_{25-100}$ ),  $4 \leq d \leq 100$  nm  
176 ( $N_{4-100}$ ),  $100 < d \leq 736$  nm ( $N_{100-736}$ ) and  $4 \leq d \leq 736$  nm ( $N_{4-736}$ ), for nucleation mode,  
177 Aitken mode, ultrafine, accumulation mode and total particles, respectively. Pearson  
178 correlation coefficient,  $r$ , was calculated by *PASW Statistics ver. 18* (SPSS Inc.) to  
179 determine the correlation between the respective parameters.

180

## 181 **2.3 Classification of new particle formation and calculation of the particle growth** 182 **and formation rates**

183 A NPF event is defined as the increase of the number concentration of nucleation  
184 mode particles, where those particles are growing into Aitken and/or accumulation  
185 mode size range ( $\geq 25$  nm) and last for a few hours until they disappear into the  
186 atmosphere by condensation or coagulation sinks (Dal Maso et al., 2005). The  
187 calculation of particle growth rate ( $GR$ ) was represented by the rate of geometric  
188 median diameter ( $GMD$ ) changes during the period of nucleation mode particles  
189 growing through 25 nm (Cheung et al., 2013). The formation rate ( $J$ ) of nucleation  
190 mode particles for each NPF event was calculated for the particle size ranging from  
191 4-25 nm according to the method of Dal Maso et al. (2005). Formation rate is defined  
192 as the sum of the apparent formation rate ( $dN_{4-25}/dt$ ) and the coagulation loss rate  
193 during the NPF event. It should be noted that the reported apparent particle formation  
194 rate is expected to be smaller than the actual nucleation rate, since some fractions of  
195 formed nuclei are always scavenged by coagulation into larger pre-existing particles  
196 before they grow larger by condensation (Lehtinen et al., 2007).

197

## 198 **2.4 Back-trajectory analysis**

199 Backward trajectories were calculated using the HYSPLIT model (Hybrid Single  
200 Particle Lagrangian Integrated Trajectory, Version 4.9) of NOAA (National Oceanic

201 and Atmospheric Administration) (Draxler, 1999) for TARO during the sampling  
202 period, in order to trace the origins of the air masses. 72-h back trajectories were  
203 calculated twice per day at 00:00LT and 12:00LT with height setting of 200 m above  
204 ground level. It should be noted that the grid resolution of the meteorological data  
205 used for back-trajectories calculation is  $1^\circ \times 1^\circ$ , which is not enough to trace the  
206 detailed air mass passage over the scale of the study region and, therefore, the  
207 trajectories only provide an indication of the region from which the air mass was  
208 originated.

209

### 210 3. *Results and discussions*

#### 211 3.1 *Particle number concentration and size distribution in respective seasons*

212 As mentioned above, the air quality of urban Taipei is significantly affected by  
213 both the local vehicular exhausts and long-range transport of pollution, where the later  
214 is dominated by meteorological factors. The information on the meteorological  
215 conditions, particularly the wind patterns, is important to elucidate our results and  
216 thus presented here. The back-trajectories of the air masses for the TARO are  
217 illustrated in **Figure 1 (left panel)**. The results showed that northeasterly winds  
218 prevailed in autumn and winter seasons, passing through the Asian continent before  
219 reaching Taiwan, whereas southerly winds prevailed in summertime. The air masses  
220 observed in spring period were found to be mainly associated with Asian continental  
221 outflows and occasionally with the southerly flows. This observation agreed with the  
222 surface wind direction measured in urban Taipei area (see **Figure 1, right panel**),  
223 where northeasterly winds were dominating during the period from November 2012  
224 to May 2013, and southerly winds were prevailing from May 2013 to August 2013.

225

226 The particle number concentrations in various size ranges during each season are  
227 summarized in **Table 1**. Relatively higher total PNCs ( $N_{4-736}$ ) were observed in spring  
228 and winter with median values of  $19.4 \times 10^3$  and  $17.4 \times 10^3 \text{ cm}^{-3}$ , respectively, followed  
229 by that of summer ( $16.6 \times 10^3 \text{ cm}^{-3}$ ) and autumn ( $13.9 \times 10^3 \text{ cm}^{-3}$ ). This result is  
230 comparable to the previous measurements conducted in urban Taipei where the  
231 seasonal means of PNCs ( $10 < d < 560\text{nm}$ ) ranged from  $11.0 \times 10^3$  to  $17.0 \times 10^3 \text{ cm}^{-3}$   
232 (Cheng et al. 2014). **Figure 2** illustrates the number, surface and volume size  
233 distributions of the aerosol particles. The geometric mean diameter (GMD) of each  
234 PSD mode was retrieved from the data of number concentration. The GMDs of the  
235 nucleation, Aitken and accumulation modes were found to be 10.4-12.8 nm, 26.5-38.4  
236 nm, and 91.8-159.0 nm, respectively.

237 In addition, the fitted GMDs of surface distribution were found to be 77.4 and  
238 293 nm for autumn, 22.1, 68.9 and 228 nm for winter, 77.4 and 253 nm for spring,

239 and 12.9 and 268 nm for summer, respectively (not shown in the figures). In winter  
240 and summer seasons, one of the fitted surface GMDs was located at nucleation mode,  
241 showing the significant contribution of nucleation mode particles in these two seasons.  
242 Bimodal volume distribution was obtained for all seasons where the fitted volume  
243 GMDs were 96.3 and 372 nm for autumn, 71.8 and 275 nm for winter, 99.5 and 339  
244 nm for spring, and 99.5 and 237 nm for summer, respectively. The GMD of first  
245 volume mode was relatively stable in each season (i.e. 71.8-99.5 nm), but smaller  
246 GMD (237 nm) for the second volume mode was observed in summer. The results  
247 implied that a higher fraction of particles could have evolved from smaller size range  
248 (i.e. nucleation and Aitken modes) into accumulation mode, which coincided with our  
249 observation that NPF events occurred mostly in summer (see Section 3.4).  
250 Furthermore, this seasonal variability agrees with our previous findings that the  
251 growth rate of newly formed particles was correlated with the photolysis of ozone, an  
252 indicator of photochemical activity (Cheung et al., 2013). The causes responsible for  
253 the observed seasonal variations in PNCs will be detailed in the following sections.

254 It was revealed that the nucleation mode particles were predominant in the PNCs  
255 during autumn, winter and spring in the study area, whereas a distinct size distribution  
256 pattern was observed in summertime. In summer, the fraction of nucleation ( $N_{4-25} /$   
257  $N_{4-736}$ ) decreased to 0.44 (see **Table 1**) and the Aitken mode PNCs increased to be  
258 comparable to that of the nucleation mode, whereas the  $N_{4-25} / N_{4-736}$  ratios for other  
259 seasons ranged from 0.56 to 0.77 (see **Table 1**). Observation from another aspect is  
260 that the PNC of nucleation mode ( $N_{4-25}$ ) peaked in winter and reached the minimum in  
261 summer, whereas the PNCs of Aitken mode ( $N_{25-100}$ ) and accumulation mode ( $N_{100-736}$ )  
262 reached their maxima in summertime. The changes in the size distribution in summer  
263 season were most likely due to the seasonally enhanced photochemical production of  
264 condensable vapors that, in turn, contributed to the growth of aerosol particles in the  
265 atmosphere.

266

### 267 **3.2 Mass concentration and chemical composition**

268 **Figures 3a** and **3b** illustrate the averaged chemical composition and mass  
269 concentration of UFPs and  $PM_{10}$ , respectively, for each season. Details of the mass  
270 concentration and chemical composition of UFPs and  $PM_{10}$  are listed in Table S1 in  
271 the appendix.

272

273 The seasonal means of UFPs ranged from 0.73 to 1.64  $\mu\text{g m}^{-3}$ , with an annual  
274 average of 1.01  $\mu\text{g m}^{-3}$ . The measured UFPs mass concentration of the present study  
275 was comparable to that in urban area of Los Angeles, United States (0.80 – 1.58  $\mu\text{g m}^{-3}$   
276  $\text{m}^{-3}$ , Hughes et al. 1998), and relatively higher than that in urban Helsinki, Finland

277 (average:  $0.49 \mu\text{g m}^{-3}$ , Pakkanen et al. 2001). For the chemical composition, organic  
278 carbon (OC) was found to be the major mass contributor, which accounted for 29.8 %  
279 (seasonal means ranging from 26.9 to 33.4 % for various seasons) of averaged mass  
280 concentration of UFPs. Elemental Carbon (EC) was the second major component with  
281 averaged mass contribution of 5.1 % (seasonal means: 2.4–7.6 %), followed by sulfate  
282 ( $\text{SO}_4^{2-}$ ) at 4.3 % (seasonal means: 3.4-6.4%) and nitrite ( $\text{NO}_2^-$ ) at 2.9% (seasonal  
283 means: 0.9-7.3%). In addition, a large fraction of mass was contributed by the group  
284 of “others”, which consisted of mineral ( $\text{K}^+$ ,  $\text{Ca}^{2+}$ ,  $\text{PO}_4^{3-}$  and  $\text{Mg}^{2+}$ ), sea-salt ( $\text{Na}^+$  and  
285  $\text{Cl}^-$ ), and unidentified species. The results showed that, on average, mineral and sea  
286 salt components attributed only 3.5 % (seasonal means: 2.0-6.0 %) to UFPs mass  
287 concentration. Thus a substantial amount of UFPs remained unidentified, which likely  
288 included hydrogen and oxygen associated with organic carbon (OC). The conversion  
289 factors used to estimate the average molecular weight per carbon in particulate  
290 organic matter varied depending on the characteristic of aerosols. A lower factor value,  
291 1.2, was usually suggested for saturated organic molecules, while a higher value, 1.6,  
292 was adopted for water-soluble compounds consisting of multifunctional oxygenated  
293 groups, and even higher factor values were suggested for aged aerosols which  
294 contained higher portion of low and semi-volatile products of photochemical reactions  
295 (Turpin and Lim et al. 2001). The high un-identified mass fraction implied that the  
296 photochemical production of secondary organic aerosols was a significant process  
297 responsible for the elevated UFPs levels observed in this study.

298

299 As shown in Fig. 3b, average  $\text{PM}_{10}$  was estimated to be  $14.7 \mu\text{g m}^{-3}$  (seasonal  
300 means:  $11.6\text{-}18.5 \mu\text{g m}^{-3}$ ) in this study, which is similar to the results of a previous  
301 study in urban Taipei (average:  $14.0 \mu\text{g m}^{-3}$ , Li et al., 2010). The measured  $\text{PM}_{10}$  level  
302 is relatively higher than that of the urban areas of Phoenix, United States ( $5.9 \mu\text{g m}^{-3}$ ,  
303 Lundgren et al. 1996) and Helsinki, Finland ( $6.1 \mu\text{g m}^{-3}$ , Vallius et al. 2000). For  
304 chemical composition, sulfate was the major mass contributor of  $\text{PM}_{10}$  (average: 39.0  
305 %, seasonal means: 33.8 - 46.8 %), followed by ammonium (average: 12.7 %, seasonal  
306 means: 12.0 - 13.2 %) and OC (average: 11.5 %, seasonal means: 9.2 to 14.3  
307 %).

308

309 The results presented above indicated that UFPs exhibited a distinct seasonal  
310 variability and composition from  $\text{PM}_{10}$  in the study area. The highest UFPs  
311 concentration was observed in summer ( $1.64 \mu\text{g m}^{-3}$ ) and the lowest in winter ( $0.73$   
312  $\mu\text{g m}^{-3}$ ). This result may be attributed to the stronger photochemical activities in  
313 summer which could have enhanced the formation of secondary organic aerosols.  
314 Consequently, the mass concentration of OC increased from  $0.20 \mu\text{g m}^{-3}$  in winter to

315 0.47  $\mu\text{g m}^{-3}$  in summertime. It is noteworthy that the mass concentration of sulfate in  
316 UFPs also peaked in summer (64  $\text{ng m}^{-3}$ ), suggesting enhancement in photo-oxidation  
317 of  $\text{SO}_2$ . Cheung et al. (2013) found that photo-oxidation of  $\text{SO}_2$  was the major  
318 mechanism for the formation of new particles in Taipei, Taiwan and the production of  
319 condensable vapors was also dominated by photo-oxidation. The co-variations in  
320 sulfate and OC revealed in this study further suggested that secondary organic  
321 compounds were the major condensable matter contributing to the growth of newly  
322 formed particles.

323

324 While the organics predominated in the mass concentration of UFPs, which  
325 included nucleation mode and Aitken mode particles, the measurements of  $\text{PM}_{10}$  in this  
326 study suggested that sulfate was the major constituent of accumulation mode aerosols.  
327 In contrast to the seasonal variation of UFPs, the mass concentration of  $\text{PM}_{10}$  reached  
328 the maximum at 18.5  $\mu\text{g m}^{-3}$  in spring and exhibited the minimum at 11.6  $\mu\text{g m}^{-3}$  in  
329 summer. The  $\text{PM}_{10}$  differences between spring and summer were mostly due to  
330 declined ambient levels of sulfate, nitrate, and ammonium ions. As a result, the mass  
331 contribution of the three inorganic ions in  $\text{PM}_{10}$  reduced from 55.7 % to 46.2 % and,  
332 on the contrary, the mass fraction of OC increased from 10.2 to 14.3 %. The seasonal  
333 characteristics of  $\text{PM}_{10}$  concentration and composition were attributed mostly to the  
334 changes in the origin areas of background air mass, which shifted from the Asia  
335 Continent to the western Pacific Ocean during summertime (see **Fig. 1**). Our previous  
336 studies reported that the fine particulate matter ( $\text{PM}_{2.5}$ ) transported on the Asian  
337 outflows to northern Taiwan maximized in springtime and were enriched in sulfate,  
338 nitrate, and ammonium (Chou et al., 2008; 2010). The seasonal variability of  $\text{PM}_{10}$   
339 found in this study was consistent with the previous observations for  $\text{PM}_{2.5}$  and  
340 thereby suggested the significance of Asian outflow aerosols to the  $\text{PM}_{10}$  budget in the  
341 downwind areas of the Asia Continent.

342

### 343 ***3.3 Seasonal characteristics of photochemical production***

344 In order to study the influences of photochemical production of particles, the  
345 measurements of PNC and PSD were analyzed per daytime (07:00 – 17:00 LT) and  
346 nighttime (17:00 – 07:00 LT), respectively (see **Figure 4**). In urban environment, the  
347 possible sources influencing the PNC and PSD are complicated, which include not  
348 only the direct emission from primary sources but also interaction between the newly  
349 formed particles, pre-existing particles and condensing vapors through the  
350 condensation and coagulation processes. Nevertheless, these processes occurred  
351 throughout the day and will not dominate in the differences between daytime and  
352 nighttime PNCs as observed in this study. It was assumed that photochemical reaction

353 was the major attributing factor to the observed diurnal differences in PNC. Since the  
354 particles in nighttime were mainly emitted from the vehicular exhausts and the  
355 elevated PNCs in daytime were due to both the primary and secondary sources of the  
356 particles in the study area (Cheung et al., 2013), a larger difference between the PNCs  
357 observed in daytime and nighttime indicated stronger influences of photochemical  
358 production on the PNCs. The most striking seasonal features shown in **Figure 4** is the  
359 large difference between daytime against nighttime PSD in summer as indicated by  
360 the low  $N_{4-736}$  (nighttime)/ $N_{4-736}$  (daytime) ratio, whereas higher ratios were observed  
361 in other seasons. In addition, the diurnal variation of particle size distribution (see  
362 **Figure 5**) provided further information about the variations in PSD. Two nucleation  
363 bursts were distinctly observed in morning and afternoon traffic peak hours in autumn,  
364 winter, and spring, while a typical PSD pattern of nucleation event (a banana curve)  
365 was dominant in summer. This result is as expected because the photochemical  
366 production of nucleation mode particles is more intense during warm seasons  
367 (Cheung et al., 2011). Moreover, as discussed in previous section, the photochemical  
368 reactions could produce condensable organics that allows the newly formed  
369 nucleation mode particles to grow into the Aitken mode. The relatively small  
370 differences between the daytime and nighttime  $N_{4-736}$  in autumn and winter indicated  
371 that the photochemical contribution in PNCs was declined as compared to that in  
372 summertime.

373

### 374 **3.4 Factors affecting new particle formation (NPF)**

375 As shown in previous study, the NPF events were frequently observed in summer,  
376 which subsequently induced a notable increase in  $N_{4-25}$  in urban Taipei (Cheung et al.  
377 2013). The frequency of NPF events was found to be 10 out of 84 measurement days  
378 and the events were observed in autumn (1 out of 23 days), spring (3 out of 26 days) and  
379 summer (6 out of 14 days) seasons. **Figure 6** (a-d) shows the scatter plots of  $N_{4-25}$   
380 against  $\text{NO}_x$  for daytimes in each season. During the NPF events, a non-linear  
381 relationship between these two parameters was usually observed during the daytime  
382 (Cheung et al. 2013). The results showed that clear NPF events were observed often  
383 in summer and occasionally in spring, but rarely in autumn and winter in the study  
384 area. The averaged particle growth and formation rates were found to be  $4.0 \pm 1.1$  nm  
385  $\text{h}^{-1}$  and  $1.4 \pm 0.8$   $\text{cm}^{-3} \text{ s}^{-1}$ , which were comparable to those measured in other urban  
386 studies in Asian cities such as Hong Kong (average:  $6.7$  nm  $\text{h}^{-1}$ , Wang et al., 2014)  
387 and Beijing (average:  $5.2$  nm  $\text{h}^{-1}$ , Wang et al., 2013). The particle growth and  
388 formation rates of each case are listed in **Table 2**.

389

390 **Table 3** summarizes the averages of  $N_{4-25}$ ,  $\text{PM}_{10}$ ,  $\text{H}_2\text{SO}_4$  proxy (as

391 UVB\*SO<sub>2</sub>/condensation sink) and wind speed for each season. The dominating  
392 factors associated to the frequent particle formation in summertime were the low  
393 PM<sub>10</sub> concentration (35.6 μg m<sup>-3</sup>) and high H<sub>2</sub>SO<sub>4</sub> proxy (493.1 ppb W m<sup>-2</sup> s). The  
394 association of sulfuric acid production and the NPF events agreed with the elevated  
395 mass concentration of sulfate in UFPs during summertime (shown in **Table S1**), as  
396 well as the results of previous urban studies (Woo et al. 2001; Cheung et al. 2013).  
397 This strongly suggested that the new particle formation was mainly driven by the  
398 photochemical oxidation of SO<sub>2</sub> under low condensation sink conditions (Gao et al.,  
399 2009; Nie et al., 2014), where the SO<sub>2</sub> could be transported from the upwind area on  
400 the summer monsoons (see **Figure 1d**). Contrarily, the absence of particle formation  
401 events in wintertime could be attributed to the declined photochemical production of  
402 H<sub>2</sub>SO<sub>4</sub> as well as suppression of NPF by particles transported from the Asian  
403 continent (Lin et al., 2004). The results of this work evidenced that low PM<sub>10</sub>  
404 concentration and high sulfuric acid production favored the particle formation process  
405 in urban areas.

406 The scatter plot between UVB\*SO<sub>2</sub> and condensation sink is depicted in **Figure**  
407 **7**. Relatively higher UVB\*SO<sub>2</sub> values were obtained during NPF events. Notably,  
408 there was a group of data with high UVB\*SO<sub>2</sub>/CS but low UVB\*SO<sub>2</sub> where no NPF  
409 event was observed. This implied that there could be a threshold level of UVB\*SO<sub>2</sub>  
410 for NPF in the study region. However, some exceptions existed in the dataset and  
411 suggested that the parameters driving NPF have not been well accounted and need to  
412 be further studied. It was also noticed that an Asian outflow event occurred on 7 April  
413 2013 during which an atypical NPF was observed (labeled as black dot in **Figure 7**).  
414 This could be relevant to the secondary particle formation on dust surface under the  
415 influence of long-range transport of air mass. This will be discussed in further details  
416 in section 3.6.

417

### 418 **3.5 Influences of local emission on PNCs**

419 Vehicle emission is known as the major source of the particulate matter in urban  
420 environment, particularly during the nighttime. In order to investigate the relationship  
421 between the vehicular exhausts and PNCs, the scatter plots of NO<sub>x</sub> (as an indicator of  
422 vehicle emission) against N<sub>4-25</sub>, N<sub>25-100</sub> and N<sub>100-736</sub> during the nighttime were  
423 examined for winter and summer periods (see **Figure 8**). The values of the Pearson  
424 correlation coefficient (*r*) and the slope of linear regression between NO<sub>x</sub> and PNCs  
425 are summarized in **Table 4**.

426

427 The highest *r* values were found in both the plots of NO<sub>x</sub> against N<sub>25-100</sub> for  
428 winter (*r* = 0.88) and summer (*r* = 0.87). This result suggested a strong linear  
429 correlation between the vehicle emission and the N<sub>25-100</sub> which coincided with the

430 results from previous studies (e.g., Morawska et al. 2008). During wintertime,  
431 stronger correlation was found between  $\text{NO}_x$  against  $\text{N}_{4-25}$  ( $r = 0.84$ ) and  $\text{N}_{25-100}$  ( $r =$   
432  $0.88$ ) compared to that between  $\text{NO}_x$  and  $\text{N}_{100-736}$  ( $r = 0.38$ ). In contrast, high  $r$  values  
433 were obtained between  $\text{NO}_x$  and all particle modes in summer ( $r = 0.70 - 0.87$ ). The  
434 robust correlation of  $\text{NO}_x$  and  $\text{N}_{4-25}$ , also  $\text{NO}_x$  and  $\text{N}_{25-100}$  suggested that local vehicle  
435 emission was the predominant source of UFPs throughout a year. These results  
436 coincided with previous studies on the size distribution of vehicle exhaust particles,  
437 which were found to be 20-130 nm and 20-60 nm, respectively, for diesel and petrol  
438 engine vehicles (Harris and Maricq 2001, Ristovski et al. 2006). However, the PNCs  
439 of accumulation mode particles ( $\text{N}_{100-736}$ ) in winter were dominated by  
440  $\text{NO}_x$ -independent sources, which were most likely related to the pollution outbreaks  
441 from the Asian continent. Lin et al. (2004) indicated that the long-range transported  
442 air mass was characterized by high level of  $\text{PM}_{10}$  and low mixing ratio of  $\text{NO}_x$  due to  
443 its short atmospheric lifetime. Interestingly, moderate correlation between the PNC of  
444 accumulation mode particles ( $\text{N}_{100-736}$ ) and  $\text{NO}_x$  was also observed in summer. Given  
445 that the Asian outflow was ceased in summertime, this correlation evidenced  
446 substantial contribution of local sources, particularly vehicular emissions, to the PNC  
447 of accumulation mode particles in Taipei, Taiwan.

448

449 The slope values can serve as a relative emission factor of particles per  $\text{NO}_x$ ,  
450 which indicates the degree of influence of vehicle emission on the PNCs (Cheung et  
451 al., 2013). The corresponding slope values for  $\text{N}_{4-25}$ ,  $\text{N}_{25-100}$ , and  $\text{N}_{100-736}$ , were found  
452 to be 279, 163, 18  $\text{cm}^{-3} \cdot \text{ppb}^{-1}$  in winter, and 239, 330, 155  $\text{cm}^{-3} \cdot \text{ppb}^{-1}$  in summer.  
453 Larger sum of slope values (724 vs. 460  $\text{cm}^{-3} \cdot \text{ppb}^{-1}$ ) was found in summertime  
454 compared to winter period, evidencing a greater influence of the vehicle emission on  
455 particle number concentration. The seasonal effects on the emission ratio of PNCs and  
456  $\text{NO}_x$  are rather difficult to address due to the complexity of different controlling  
457 factors, such as formation mechanisms and meteorological conditions. For example,  
458 Nam et al. (2010) reported negatively exponential correlation between the  $\text{PM}/\text{NO}_x$   
459 ratio in vehicle emission and ambient temperature, and suggested that the impact of  
460 ambient temperature on particulate matter was larger than that on  $\text{NO}_x$ . Nevertheless,  
461 the observed differences in the PNCs/ $\text{NO}_x$  ratios for winter and summer periods of  
462 this study necessitate further investigations on the formation mechanisms of aerosol  
463 particles in urban areas, in particular the nucleation and the Aitken modes.

464

### 465 ***3.6 Influence of long-range transport (LRT)***

466 During the seasons of winter monsoons, i.e. from autumn to spring, the  
467 continental outflows have been frequently observed in urban Taipei, which is

468 indicated by the stable northeasterly wind and increase of O<sub>3</sub> level (Lin et al. 2004).  
469 Previous studies of long-range transport (LRT) of air pollutants on air quality of  
470 northern Taiwan showed that an elevated PM<sub>10</sub> was observed under the influence of  
471 continental outflows (Lin et al., 2004, Chou et al., 2004). **Figure 9** depicts an LRT  
472 pollution event observed at the TARO during this study. The wind direction changed  
473 from westerly/northwesterly to northeasterly at 21:00, 24 March which continued  
474 until 06:00, 26 March. During this period, the O<sub>3</sub> mixing ratio remained at moderate  
475 level (~30-55 ppb) and PM<sub>10</sub> increased from 10.0 to 98.0 µg m<sup>-3</sup>. It should be noted  
476 that the variations of measured pollutants were not solely influenced by the  
477 long-range transport, but also partly due to the variation of local pollution and  
478 boundary dynamics. In this section, we attempt to analyze the PSD/PNC under the  
479 influences of continental pollution outbreaks. The periods of the respective LRT  
480 events are listed in **Table S2**.

481

482 As shown in **Figure 9**, the diurnal variations of PSD during the LRT event  
483 exhibited two N<sub>4-25</sub> peaks associated to the morning and afternoon traffic rush hours,  
484 whereas the PNCs of the Aitken mode particles remained at a low level. The results  
485 suggested that the influences of local vehicle emission on PNCs were still in place,  
486 whereas growth of particles due to secondary production of condensable vapors could  
487 have been suppressed, as NPF was rarely observed during the LRT events. It is  
488 noteworthy that a weak dust transport event was observed on 7 April 2013 where a  
489 banana shape was observed in the PSD, evidencing that secondary formation of  
490 particles could have had occurred. However, the dominating diameter of particles was  
491 ~ 40-50 nm at the initial stage of the event. The banana shape of PSD data was  
492 initiated since ~06:00 LT until 21:00 LT, when the northeasterly wind prevailed. The  
493 PM<sub>10</sub> and O<sub>3</sub> increased from minima of 44 µg m<sup>-3</sup> (at 06:00 LT) and 25 ppb (at 05:00  
494 LT) to the daily maxima of 92 µg m<sup>-3</sup> (at 17:00 LT) and 61 ppb (at 16:00 LT). This  
495 result showed that the NPF process could have occurred in the upwind area where  
496 newly formed particles were transported to the study site, or heterogeneously formed  
497 particles were released from the dust surface during the long-range transport of air  
498 pollutants (Nie et al., 2014).

499

500 The averaged PSDs for LRT and non-LRT cases are shown in **Figure 10**. The  
501 geometric mean diameters of the nucleation, Aitken, and accumulation modes in PSD  
502 were found to be 10.6, 37.2 and 156.8 nm for LRT and 11.3, 30.0 and 113.4 nm for  
503 non-LRT cases, respectively. The median N<sub>4-25</sub> (11.1x10<sup>3</sup> cm<sup>-3</sup>), N<sub>25-100</sub> (7.3x10<sup>3</sup> cm<sup>-3</sup>)  
504 and N<sub>100-736</sub> (1.8x10<sup>3</sup> cm<sup>-3</sup>) observed in non-LRT events were significantly higher than  
505 those for LRT events (N<sub>4-25</sub>: 9.2x10<sup>3</sup> cm<sup>-3</sup>, N<sub>25-100</sub>: 3.8x10<sup>3</sup> cm<sup>-3</sup>, N<sub>100-736</sub>: 1.3x10<sup>3</sup> cm<sup>-3</sup>).

506 This was attributed to the lower average wind speed (and hence poor dispersion)  
507 during non-LRT events ( $1.5\pm 0.8 \text{ m s}^{-1}$ ) than that for LRT events ( $3.0\pm 0.8 \text{ m s}^{-1}$ ). In  
508 contrast to the increase in  $\text{PM}_{10}$  observed usually during LRT episodes (e.g., Lin et al.,  
509 2012), the relatively lower PNCs suggested that the number concentration of  
510 submicron particles, in particular UFPs, was dominated by local emissions during the  
511 episodes of continental pollution outbreaks. This agreed with the observation of  
512 seasonal UFPs mass concentration that peaked in summertime when Taiwan was  
513 isolated from the influences of continental air mass.

514

#### 515 **4. Conclusions**

516 The mass concentration and chemical composition of ultrafine particles (UFPs)  
517 and submicron particles (i.e.  $\text{PM}_{1}$ ) as well as the particle number concentration (PNC)  
518 and size distributions (PSD) with size ranging from 4 to 736 nm were measured  
519 during four seasonal campaigns in the period from October 2012 to August 2013 at  
520 the TARO, a subtropical urban aerosol station in Taipei, Taiwan. Significant seasonal  
521 variability and chemical composition of UFPs and  $\text{PM}_{1}$  were revealed. The UFPs  
522 were composed mostly of organic matter and reached maxima in summer, whereas the  
523  $\text{PM}_{1}$  composition was dominated by ammonium and sulfate and exhibited a seasonal  
524 peak in spring.

525

526 It was found that the total PNC was significantly elevated during cold seasons,  
527 which was caused mostly by the high level of nucleation mode particles ( $\text{N}_{4-25}$ ). On  
528 the contrary, both the Aitken mode ( $\text{N}_{25-100}$ ) and accumulation mode ( $\text{N}_{100-736}$ ) PNCs  
529 reached their respective maxima in summertime. Consistent correlation without  
530 significant seasonal variations was found between the UFPs (i.e. nucleation and  
531 Aitken mode particles) and  $\text{NO}_x$ , suggesting that local vehicle emission was the major  
532 source of UFPs in the study area throughout a year. The local vehicle emission was  
533 also dominating the accumulation mode PNC in summer, but not in wintertime. The  
534 declined correlation between  $\text{NO}_x$  and  $\text{N}_{100-736}$  in winter ( $r = 0.38$ ) was likely due to  
535 the influences of air pollution associated with the Asian outflows.

536

537 The elevated UFPs level in summer was attributed to the increase in the  
538 concentration of Aitken mode particles ( $\text{N}_{25-100}$ ). It was revealed from the  
539 measurements of PSD that a large number of nucleation mode particles could have  
540 evolved into the Aitken mode during summertime, which was most likely relevant to  
541 the photochemical production of condensable vapors that, in turn, could have  
542 contributed to the growth of particles in the atmosphere. Moreover, the chemical  
543 measurements suggested that the constituents of the condensed materials in UFPs

544 were mostly organic matter, implying the significance of secondary organic aerosols  
545 in the ambient UFPs.

546

547 A total of 10 new particle formation (NPF) events occurred out of 84  
548 measurement days in this study, which were observed in autumn (1 out of 23 days),  
549 spring (3 out of 26 days) and summer (6 out of 14 days) seasons. The prevalence of  
550 NPF in summer agreed with the highest H<sub>2</sub>SO<sub>4</sub> proxy and lowest PM<sub>10</sub> observed in  
551 this study, which provided favorable atmospheric conditions for new particle  
552 formation. The averaged particle growth and formation rates for the NPF events were  
553  $4.0 \pm 1.1 \text{ nm h}^{-1}$  and  $1.4 \pm 0.8 \text{ cm}^{-3} \text{ s}^{-1}$ , respectively, which were comparable to those  
554 measured in previous urban studies.

555

556 As exemplifying above, the characteristics of various physicochemical properties  
557 of particles investigated in this study and the occurrence of NPF exhibited a strong  
558 seasonal variability, which was co-influenced by the long-range transported particles  
559 during the seasons of winter monsoons and the strong photochemical activities in  
560 summer. The results of this study are critical for the authorities involved in urban  
561 development and health impact assessment, and the environmental policy makers who  
562 are tackling the severe atmospheric pollution in the East Asia region.

563

#### 564 *Acknowledgements*

565 This research was supported by the Academia Sinica and the Ministry of Science and  
566 Technology of Taiwan through grants 103-2111-M-001-003, 102-2628-M-001-007,  
567 and 101-2119-M-001-003. The authors thank the Taiwan EPA for providing the air  
568 quality and meteorological data. We also thank the Department of Atmospheric  
569 Science of National Taiwan University for the logistical supports to the operation of  
570 TARO. Prof. Tareq Hussein is gratefully acknowledged for providing us the code of  
571 DO-FIT.

572

573 **Table 1.** Median and standard deviation of the PNCs measured in each season. The size  
574 ranges of the PNCs were represented by the subscripted number. For example,  $N_{4-25}$ ,  
575 represents the number concentrations of the particles from 4 to 25 nm. The fractions of  $N_{4-25}$   
576 and  $N_{4-100}$  to total PNCs were presented in the last two columns.

577

	<i>Measurement periods</i>	$N_{4-736}$ (#/cm <sup>3</sup> )	$N_{4-25}$ (#/cm <sup>3</sup> )	$N_{25-100}$ (#/cm <sup>3</sup> )	$N_{4-100}$ (#/cm <sup>3</sup> )	$N_{100-736}$ (#/cm <sup>3</sup> )	$N_{4-25}/N_{4-736}$	$N_{4-100}/N_{4-736}$
<i>Autumn</i>	24 Oct–15 Nov 2012	13.9 x 10 <sup>3</sup> (6.7x10 <sup>3</sup> )	8.6 x 10 <sup>3</sup> (4.5x10 <sup>3</sup> )	3.9 x 10 <sup>3</sup> (2.7x10 <sup>3</sup> )	12.7 x 10 <sup>3</sup> (6.4x10 <sup>3</sup> )	1.3 x 10 <sup>3</sup> (0.9x10 <sup>3</sup> )	0.62	0.90
<i>Winter</i>	4–24 Jan 2013	17.4 x 10 <sup>3</sup> (8.7x10 <sup>3</sup> )	11.6 x 10 <sup>3</sup> (6.0x10 <sup>3</sup> )	4.1 x 10 <sup>3</sup> (3.7x10 <sup>3</sup> )	16.3 x 10 <sup>3</sup> (8.5x10 <sup>3</sup> )	0.9 x 10 <sup>3</sup> (0.9x10 <sup>3</sup> )	0.70	0.94
<i>Spring</i>	17 Mar–11 Apr 2013	19.4 x 10 <sup>3</sup> (13.8x10 <sup>3</sup> )	10.3 x 10 <sup>3</sup> (11.3x10 <sup>3</sup> )	5.8 x 10 <sup>3</sup> (4.3x10 <sup>3</sup> )	17.0 x 10 <sup>3</sup> (13.6x10 <sup>3</sup> )	1.9 x 10 <sup>3</sup> (1.1x10 <sup>3</sup> )	0.56	0.89
<i>Summer</i>	1–14 Aug 2013	16.6 x 10 <sup>3</sup> (16.4x10 <sup>3</sup> )	6.9 x 10 <sup>3</sup> (9.1x10 <sup>3</sup> )	6.0 x 10 <sup>3</sup> (9.1x10 <sup>3</sup> )	13.7 x 10 <sup>3</sup> (15.4x10 <sup>3</sup> )	3.1 x 10 <sup>3</sup> (2.6x10 <sup>3</sup> )	0.44	0.87

578

579 **Table 2.** Time periods defined as the new particle formation events and the particle growth  
 580 and formation rates

<i>Date</i>	<i>Time period (LT)</i>	<i>Growth rate (nm h<sup>-1</sup>)</i>	<i>Formation rate (cm<sup>-3</sup> s<sup>-1</sup>)</i>
9 Nov 2012	07:00-13:00	3.4	1.30
26 Mar 2013	06:00-10:00	3.4	1.91
4 Apr 2013	07:00 – 10:00	3.7	1.13
5 Apr 2013	08:00 – 12:00	5.5	1.10
4 Aug 2013	09:00 – 12:00	3.9	1.84
5 Aug 2013	09:00 – 13:00	4.9	2.44
7 Aug 2013	06:00 – 12:00	3.5	0.84
8 Aug 2013	09:00 – 12:00	5.0	2.76
9 Aug 2013	06:00 – 13:00	1.6	0.39
11 Aug 2013	06:00 – 09:00	4.8	0.58
Average		4.0 (±1.1)	1.4 (±0.8)

581

582

583 **Table 3.** Average of  $N_{4-25}$ ,  $PM_{10}$ , UVB,  $SO_2$ , condensation sink (CS),  $H_2SO_4$  proxy and wind  
 584 speed of different seasons. (note: the data with observation of rainfall was not used in  
 585 calculation).

<i>Periods</i>	<i><math>N_{4-25}</math></i> <i>(<math>cm^{-3}</math>)</i>	<i><math>PM_{10}</math></i> <i>(<math>\mu g m^{-3}</math>)</i>	<i>UVB</i> <i>(<math>Wm^{-2}</math>)</i>	<i><math>SO_2</math></i> <i>(ppb)</i>	<i>CS</i> <i>(<math>10^{-2} s^{-1}</math>)</i>	<i><math>H_2SO_4</math> proxy</i> <i>(ppb <math>Wm^{-2} s</math>)</i>	<i>Wind speed</i> <i>(<math>ms^{-1}</math>)</i>
Autumn	$8.6 \times 10^3$	53.9	1.04	2.27	0.85	307.1	2.82
Winter	$11.6 \times 10^3$	48.4	0.80	2.58	0.75	240.0	2.34
Spring	$10.5 \times 10^3$	61.1	0.99	2.76	1.35	238.4	2.17
Summer	$6.9 \times 10^3$	35.6	1.97	3.19	1.89	493.1	2.35

586

587 **Table 4.** Pearson correlation coefficient ( $r$ ) and slope of linear regression of PNCs against  
 588  $\text{NO}_x$  during the nighttime (20:00-04:00 LT) in winter and summer periods.

<i>Periods</i>		$N_{4-25}$	$N_{25-100}$	$N_{100-736}$
Winter	<i>Slope</i>	279	163	18
	$r$	0.84	0.88	0.38
Summer	<i>Slope</i>	239	330	155
	$r$	0.76	0.87	0.70

589

590 **References**

- 591 Charlson, R.J., Schwartz, S.E., Hales, J.M., Cess, R.D., Coakley Jr., J.A., Hansen, J.E.  
592 and Hofmann, D.J. (1992). Climate forcing by anthropogenic aerosols. *Science*, 255,  
593 423-430.
- 594 Cheng, Y.-H., Kao, Y.-Y. and Liu, J.-J. (2014). Correlations between black carbon  
595 mass and size-resolved particle number concentrations in the Taipei urban area: A  
596 five-year long-term observation. *Atmospheric Pollution Research*, 5, 62-72.
- 597 Cheung, H.C., Wang, T., Baumann, K. and Guo, H. (2005). Influence of regional  
598 pollution outflow on the concentrations of fine particulate matter and visibility in the  
599 coastal area of southern China. *Atmospheric Environment*, 39, 6463-6474.
- 600 Cheung, H.C., Morawska, L. and Ristovski, Z.D. (2011). Observation of new particle  
601 formation in subtropical urban environment. *Atmospheric Chemistry and Physics*, 11,  
602 3823-3833.
- 603 Cheung, H.C., Chou, C.C.-K., Huang, W.-R. and Tsai, C.-Y. (2013). Characterization  
604 of ultrafine particle number concentration and new particle formation in an urban  
605 environment of Taipei, Taiwan. *Atmospheric Chemistry and Physics*, 13, 8935-8946.
- 606 Chou, C. C.-K., Lee, C. T., Cheng, M. T., Yuan, C. S., Chen, S. J., Wu, Y. L., Hsu, W.  
607 C., Lung, S. C., Hsu, S. C., Lin, C. Y., Liu, S. C. (2010). Seasonal variations and  
608 spatial distribution of carbonaceous aerosols in Taiwan, *Atmos. Chem. Phys*, 10,  
609 9563–9578.
- 610 Chou, C. C.-K., Lee, C.-T., Yuan, C. S., Hsu, W. C., Hsu, S. C., Liu, S. C. (2008).  
611 Implications of the chemical transformation of Asian outflow aerosols for the  
612 long-range transport of inorganic nitrogen species. *Atmospheric Environment*, 42,  
613 7508-7519.
- 614 Chou, C. C.-K., Huang, S.-H., Chen, T.-K., Lin, C.-Y. and Wang, L.-C. (2005).  
615 Size-segregated characterization of atmospheric aerosols in Taipei during Asian  
616 outflow episodes. *Atmospheric Research*, 75, 89-109.
- 617 Chou, C. C.-K., Lin, C.-Y., Chen, T.-K., Hsu, S.-C., Lung, S.-C., Liu, S.C. and Young,  
618 C.-Y. (2004). Influence of Long-Range Transport Dust Particles on Local Air  
619 Quality: A Case Study on Asian Dust Episodes in Taipei during the Spring of 2002.  
620 *Terrestrial, Atmospheric and Oceanic Sciences*, 15, 881-889.
- 621 Chow, J. C., Watson, J. G., Chen, L.-W. A., Chang, L.C.O., Robinson, N. F., Trimble,  
622 D. and Kohl, S. (2007). The IMPROVE\_A Temperature Protocol for  
623 Thermal/Optical Carbon Analysis: Maintaining Consistency with a Long-Term  
624 Database, *Journal of the Air & Waste Management Association*, 57:9, 1014-1023.
- 625 Dal Maso, M., Kulmala, M., Riipinen, I., Wagner, R., Hussein, T., Aalto, P.P. and  
626 Lehtinen, K.E.J. (2005). Formation and growth of fresh atmospheric aerosols: eight  
627 years of aerosol size distribution data from SMEAR II, Hyytiälä, Finland. *Boreal*

628 Environ. Res., 10, 323-336.

629 Donaldson, K., Li, X.Y. and MacNee, W (1998). Ultrafine (nanometre) particle  
630 mediated lung injury. *Journal of Aerosol Science*, 29, 553, 560.

631 Draxler, R.R. (1999). HYSPLIT4 user's guide. NOAA Tech. Memo. ERL ARL-230,  
632 NOAA Air Resources Laboratory, Silver Spring, MD.

633 Gao, J., Wang, T., Zhou, X. Wu, W. and Wang, W. (2009). Measurement of aerosol  
634 number size distributions in the Yangtze River delta in China: Formation and growth  
635 of particles under polluted conditions. *Atmos. Environ.*, 43, 829-836.

636 Guo, H., Ding, A., Morawska, L., He, C., Ayoko, G., Li, Y. and Hung, W. (2008). Size  
637 distribution and new particle formation in sub-tropical eastern Australia.  
638 *Environmental Chemistry*, 5, 382-390.

639 Harris, S.J. and Maricq, M.M. (2001). Signature size distributions for diesel and  
640 gasoline engine exhaust particulate matter. *Journal of Aerosol Science*, 32, 749-764.

641 Holman, J.P. (1972). *Heat Transfer*. New York, McGraw-Hill.

642 Holmes, N.S. (2007). A review of particle formation events and growth in the  
643 atmosphere in the various environments and discussion of mechanistic implications.  
644 *Atmospheric Environment*, 41, 2183-2201.

645 Hsu, S.-C., Lee, C.S.L., Huh, C.-A., Shaheen, R., Lin, F.-J. and Liu, S.C. (2014).  
646 Ammonium Deficiency Caused by Heterogeneous Reactions during a Super Asian  
647 Dust Episode. *Journal of Geophysical Research*, 119(11),  
648 doi:10.1002/2013JD021096.

649 Hughes, L.S., Cass, G.R., Gone, J., Ames, M. and Olmez, I. (1998). Physical and  
650 Chemical Characterization of Atmospheric Ultrafine Particles in the Los Angeles  
651 Area. *Environmental Science and Technology*, 32, 1153-1161.

652 Hussein, T., Dal Maso, M., Petäjä, T., Koponen, I.K., Paatero, P., Aalto, P.P., Hämeri,  
653 K. and Kulmala, M. (2005). Evaluation of an automatic algorithm for fitting the  
654 particle number size distributions. *Boreal Env. Res.* 10:337-355.

655 Juwono, A., Johnson, G.R., Mazaheri, M. and Morawska, L., Roux, F. and Kitchen, B.  
656 (2013). Investigation of the airborne submicrometer particles emitted by dredging  
657 vessels using a plume capture method. *Atmospheric Environment*, 73, 112-123.

658 Kulmala, M. (2003). How Particles Nucleate and Grow. *Science*, 302, 1000-1001.

659 Kulmala, M., Kontkanen, J., Junninen, H., Lehtipalo, K., Manninen, H.E., Nieminen,  
660 T., Petäjä, T., Sipilä, M., Schobesberger, S., Rantala, P., Franchin, A., Jokinen, T.,  
661 Järvinen, E., Äijälä, M., Kangasluoma, J., Hakala, J., Aalto, P.P., Paasonen, P.,  
662 Mikkilä, J., Vanhanen, J., Aalto, J., Hakola, H., Makkonen, U., Ruuskanen, T.,  
663 Mauldin III, R.L., Duplissy, J., Vehkamäki, H., Bäck, J., Kortelainen, A., Riipinen I.,  
664 Kurtén, T., Johnston, M.V., Smith, J.N., Ehn, M., Mentel, T.F., Lehtinen, K.E.J.,  
665 Laaksonen, A., Kerminen, V.-M. and Worsnop, D.R. (2013). Direct Observations of

666 Atmospheric Aerosol Nucleation. *Science*, 339, 943-946.

667 Kulmala, M., Petäjä, T., Nieminen, T., Sipilä, M., Manninen, H.E., Lehtipalo, K., Dal  
668 Maso, M., Aalto, P.P., Junninen, H., Paasonen, P., Riipinen, I., Lehtinen, K.E.,  
669 Laaksonen, A. and Kerminen, V.-M. (2012). Measurement of the nucleation of  
670 atmospheric aerosol particles. *Nature Protocols*, 7, 1651-1667.

671 Kulmala, M., Vehkamäki, H., Petäjä, T., Dal Maso, M., Lauri, A., Kerminen, V.-M.,  
672 Birmili, W. and McMurry, P.H. (2004). Formation and growth rates of ultrafine  
673 atmospheric particles: a review of observations. *Journal of Aerosol Science*, 35,  
674 143-176.

675 Lehtinen, K.E.J., Dal Maso, M., Kulmala, M. and Kerminen, V.-M. (2007).  
676 Estimating nucleation rates from apparent particle formation rates and vice versa:  
677 Revised formulation of the Kerminen-Kulmala equation. *J. Aerosol Sci.*, 38,  
678 988-994, doi:10.1016/j.jaerosci.2007.06.009.

679 Li, C.-S. and Lin, C.-H. (2010). PM<sub>1</sub>/PM<sub>2.5</sub>/PM<sub>10</sub> Characteristics in the Urban  
680 Atmosphere of Taipei. *Aerosol Science and Technology*, 36:4, 469-473.

681 Lin, C.-Y., Liu, S.C., Chou, C.C.-K., Liu, T.H. and Lee, C.-T. (2004). Long-Range  
682 Transport of Asian Dust and Air Pollutants to Taiwan. *Terr. Atmos. and Ocean. Sci.*,  
683 15, 759-784.

684 Lin, C.-Y., Chou, C. C.-K., Wang, Z., Lung, S.-C., Lee, C.-T., Yuan, C.-S., Chen,  
685 W.-N., Chang, S.-Y., Hsu, S.-C., Chen, W.-C. and Liu, S. C. (2012). Impact of  
686 different transport mechanisms of Asian dust and anthropogenic pollutants to Taiwan.  
687 *Atmos. Environ.*, 60, 403-418.

688 Lundgren, D.A. Hlaing, D.N., Rich, T.A. and Marple, V.A. (1996). PM<sub>10</sub>/PM<sub>2.5</sub>/PM<sub>1</sub>  
689 Data from a Trichotomous Sampler. *Aerosol Science and Technology*, 25, 353-357.

690 Marple, V. A., Rubow, K. L. and Behm, S. M. (1991). A Microorifice Uniform  
691 Deposit Impactor (MOUDI): Description, Calibration, and Use, *Aerosol Science and*  
692 *Technology*, 14:4, 434-446.

693 Matsumoto, K., Uyama, Y., Hayano, T., Tanimoto, H., Uno, Itsushi. and Uematsu, M.  
694 (2003). Chemical properties and outflow patterns of anthropogenic and dust  
695 particles on Rishiri Island during the Asian Pacific Regional Aerosol  
696 Characterization Experiment (ACE-Asia). *Journal of Geophysical Research*, 108  
697 (D23), 8666, doi:10.1029/2003JD003426.

698 Mazaheri, M., Johnson, G.R. and Morawska, L. (2009). Particle and Gaseous  
699 Emissions from Commercial Aircraft at Each Stage of the Landing and Takeoff  
700 Cycle. *Environmental Science and Technology*, 43, 441-446.

701 Morawska, L., Ristovski, Z., Jayaratne, E.R., Keogh, D.U. and Ling, X. (2008).  
702 Ambient nano and ultrafine particles from motor vehicle emissions: Characteristics,  
703 ambient processing and implications on human exposure. *Atmospheric Environment*,

704 42, 8113-8138.

705 Nam, E., Kishan, S., Baldauf, R.W., Fulper, C.R., Sabisch, M. and Warila, J. (2010).  
706 Temperature Effects on Particulate Matter Emissions from Light-Duty,  
707 Gasonline-Powered Motor Vehicles. *Environmental Science and Technology*, 44,  
708 4672-4677.

709 Nie, W., Ding, A., Wang, T., Kerminen, V.-M., George, C., Xue, L., Wang, W., Zhang,  
710 Q., Petäjä, T., Qi, X., Gao, Xiaomei, Wang, X., Yang, X., Fu, C. and Kulmala.  
711 (2014). Polluted dust promotes new particle formation and growth. *Scientific*  
712 *Reports*, 4, 6634.

713 Pakkanen, T.A., Kerminen, V.-M., Korhonen, C.H., Hillamo, R.E., Aarnio, P.,  
714 Koskentalo, T. and Maenhaut, W. (2001). Urban and rural ultrafine (PM<sub>0.1</sub>) particles  
715 in the Helsinki area. *Atmospheric Environment*, 35, 4593-4607.

716 Pérez, N., Pey, J., Cusack, M., Reche, C., Querol, X., Alastuey, A. and Viana, M  
717 (2010). Variability of Particle Number, Black Carbon, and PM<sub>10</sub>, PM<sub>2.5</sub> and PM<sub>1</sub>  
718 Levels and Speciation: Influence of Road Traffic Emissions on Urban Air Quality.  
719 *Aerosol Science and Technology*, 44, 487-499.

720 Pey, J., Rodríguez, S., Querol, X., Alastuey, A., Moreno, T., Putaud, J.P., and Van  
721 Dingenen, R (2008). Variations of urban aerosols in the western Mediterranean.  
722 *Atmospheric Environment*, 42, 9052-9062.

723 Pey, J., Querol, X., Alastuey, A., Rodriguez, S., Putaud, J.P. and Van Dingenen, R.  
724 (2009). Source apportionment of urban fine and ultrafine particle number  
725 concentration in a Western Mediterranean city. *Atmospheric Environment*, 43,  
726 4407-4415.

727 Reche, C., Querol, X., Alastuey, A., Viana, M., Pey, J., Moreno, T., Rodríguez, S.,  
728 González, Y., Fernández-Camacho, R., de la Rosa, J., Dall'Osto, M., Prévôt, A.S.H.,  
729 Hueglin, C., Harrison, R.M. and Quincey, P. (2011). New considerations for PM,  
730 Black Carbon and particle number concentration for air quality monitoring across  
731 different European cities. *Atmospheric Chemistry and Physics*, 11, 6207-6227, 2011.

732 Ristovski, Z.D., Jayaratne, E.R., Lim, M., Ayoko, G.A. and Morawska, L. (2006).  
733 Influence of diesel fuel sulphur on the nanoparticle emissions from city buses.  
734 *Environmental Science and Technology*, 40, 1314-1320.

735 Salvador, C.M. and Chou, C.C.-K. (2014). Analysis of semi-volatile materials (SVM)  
736 in fine particulate matter. *Atmospheric Environment*, 95, 288-295.

737 Subramanian, R., Khlystov, A.Y., Cabada, J.C. and Robinson, A.L. (2004). Positive  
738 and negative artifacts in particulate organic carbon measurements with denuded and  
739 undenuded sampler configurations. *Aerosol Science and Technology*, 38, 27-48.

740 Turpin, B.J. and Lim, H.-J. (2001). Species contributions to PM<sub>2.5</sub> mass  
741 concentrations: revisiting common assumptions for estimating organic mass. *Aerosol*

742 Science and Technology, 35, 602-610.

743 Vallius, M.J. Ruuskanen, J. Mirme, A. and Pekkanen, J. (2000). Concentrations and  
744 Estimated Soot Content of PM<sub>1</sub>, PM<sub>2.5</sub> and PM<sub>10</sub> in a Subarctic Urban Atmosphere.  
745 Environmental Science and Technology, 34, 1919-1925.

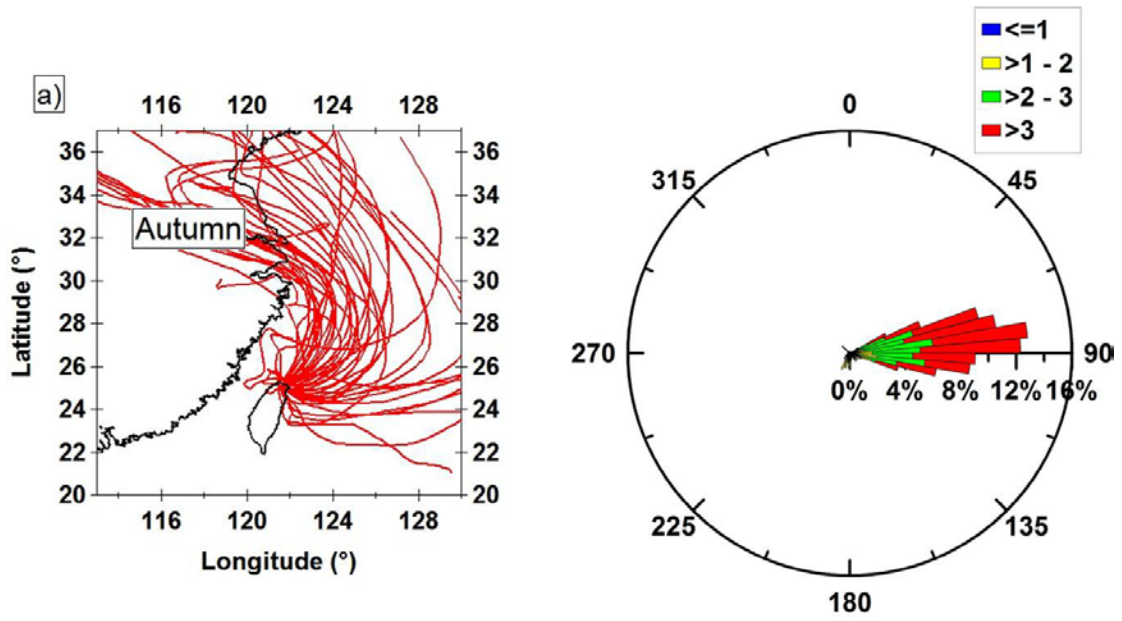
746 Wang, T., Ding, A.J., Blake, D.R., Zahorowski, W., Poon, C.N. and Li, Y-S. (2003).  
747 Chemical characterization of the boundary layer outflow of air pollution to Hong  
748 Kong during February-April 2001.

749 Wang, D., Guo, H., Cheung, K. and Gan, F. (2014). Observation of nucleation mode  
750 particle burst and new particle formation events at an urban site in Hong Kong.  
751 Atmospheric Environment, 99, 196-205.

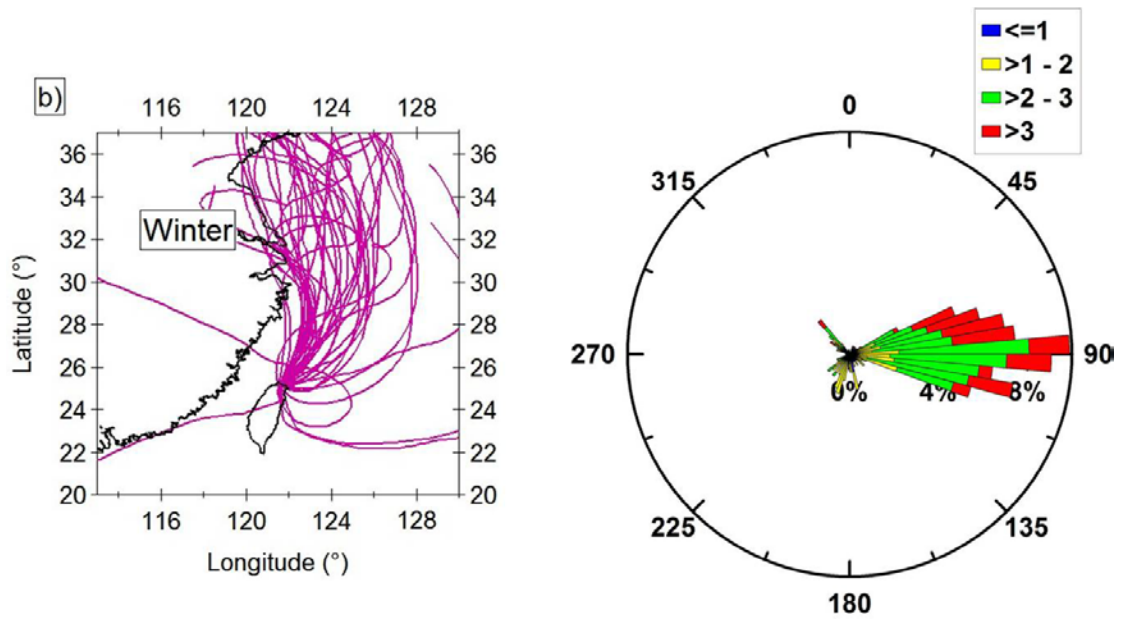
752 Wang Z. B., Hu, M., Suu, J.Y., Wu, Z.J., Yue, D.L., Shen, X.J., Zhang, Y.M., Pei, X.Y.,  
753 Cheng, Y.F. and Wiedensohler, A. (2013). Characteristics of regional new particle  
754 formation in urban and regional background environments in the North China Plain.  
755 Atmospheric Chemistry and Physics, 13, 12495-12506.

756 Woo, K.S., Chen, D.R., Pui, D.Y.H. and McMurry, P.H. (2001). Measurement of  
757 Atlanta aerosol size distribution: observation of ultrafine particle events. Aerosol  
758 Science and Technology, 34, 75-87.

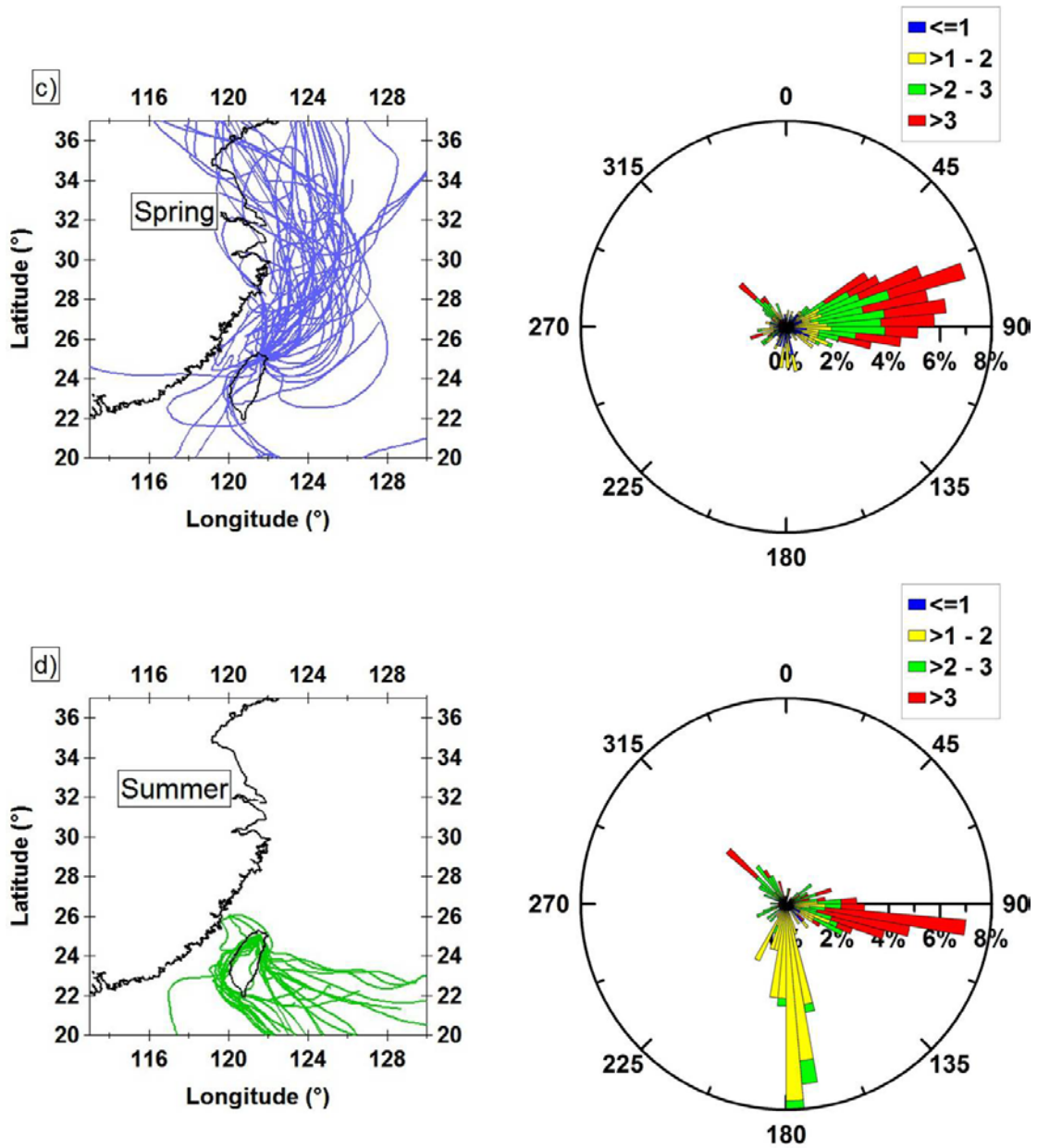
759



760



761



762

763

764

765 **Figure 1.** Back-trajectories calculated for TARO for the measurement periods (left panel) and

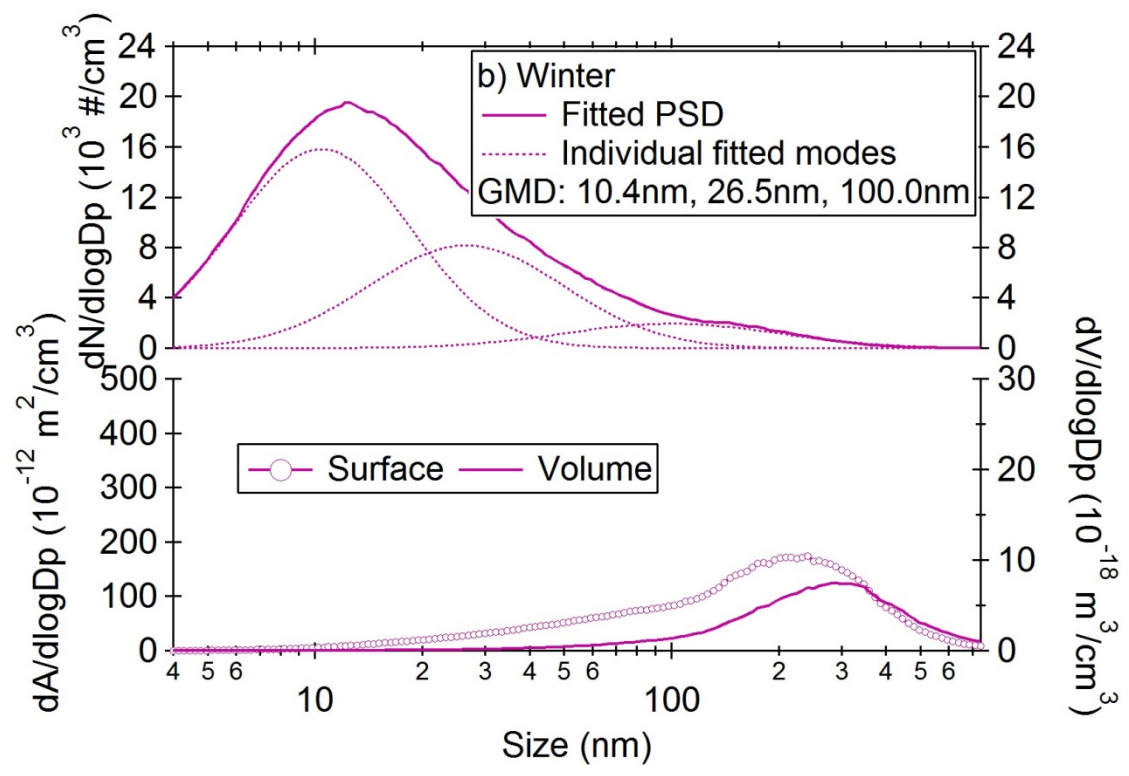
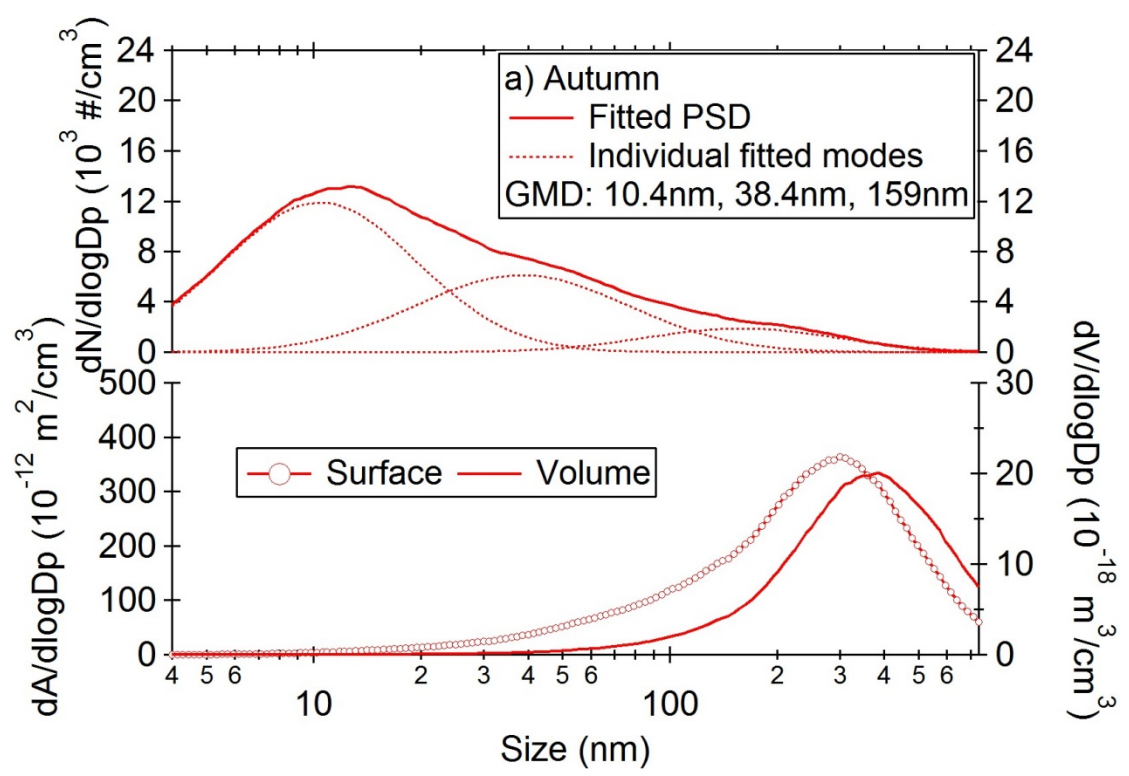
766 surface wind rose plots (right panel) in (a) autumn, (b) winter, (c) spring and (d) summer. The

767 color codes of wind rose plots represent the wind speed: blue  $< 1 \text{ ms}^{-1}$ ; yellow  $1-2 \text{ ms}^{-1}$ ; green

768  $2-3 \text{ ms}^{-1}$ ; and red  $> 3 \text{ ms}^{-1}$ .

769

770  
771  
772  
773  
774  
775  
776  
777  
778  
779  
780  
781  
782  
783  
784  
785  
786  
787  
788  
789  
790  
791  
792  
793  
794  
795  
796  
797  
798  
799  
800  
801  
802  
803  
804  
805  
806  
807  
808  
809  
810  
811  
812  
813  
814  
815  
816  
817  
818  
819  
820  
821



822  
823  
824  
825  
826  
827  
828  
829  
830  
831  
832  
833  
834  
835  
836  
837  
838  
839  
840  
841  
842  
843  
844  
845  
846  
847  
848  
849  
850  
851  
852  
853  
854  
855  
856  
857  
858  
859  
860  
861  
862  
863  
864  
865  
866  
867  
868  
869  
870  
871  
872  
873  
874  
875  
876

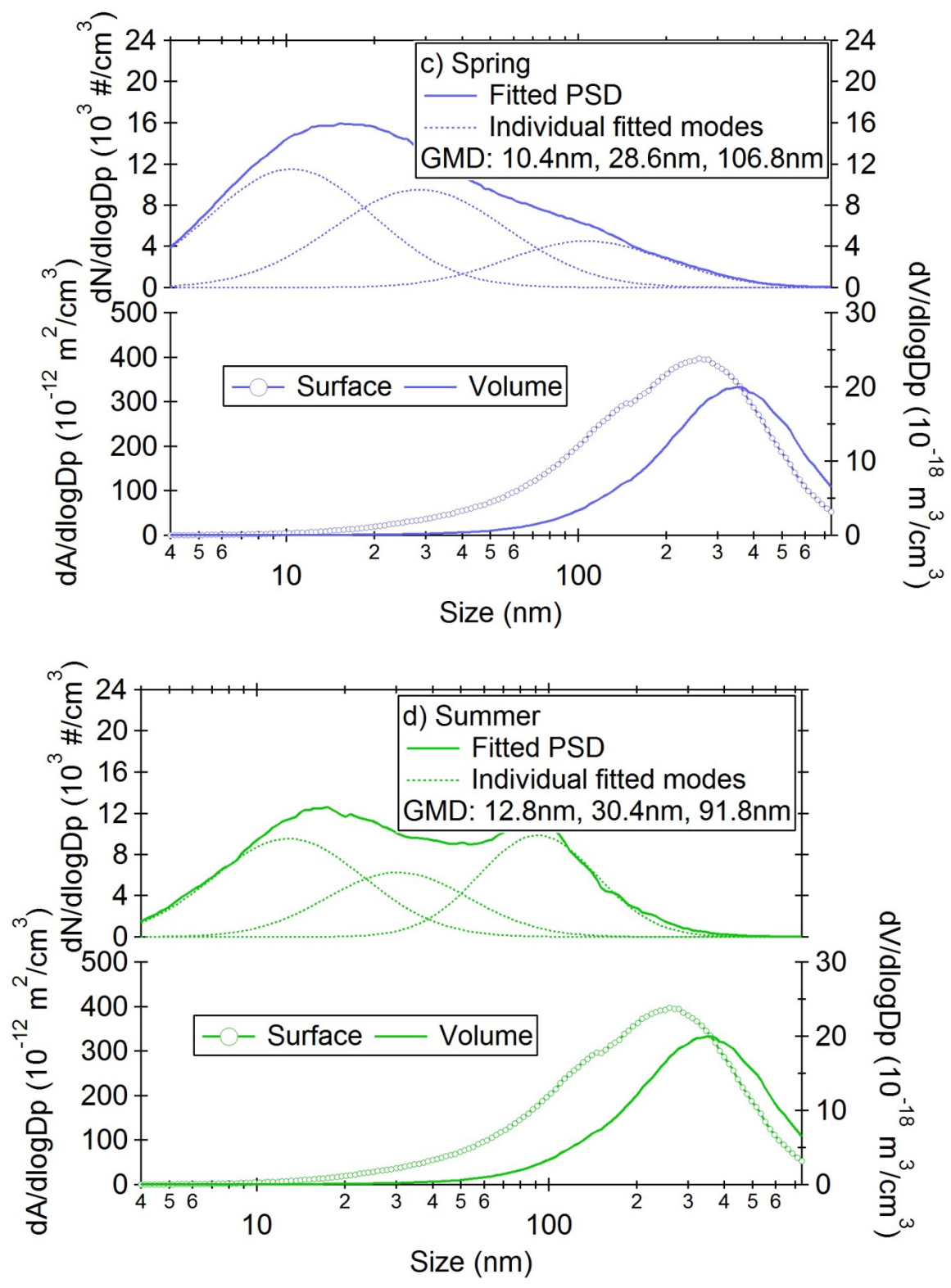
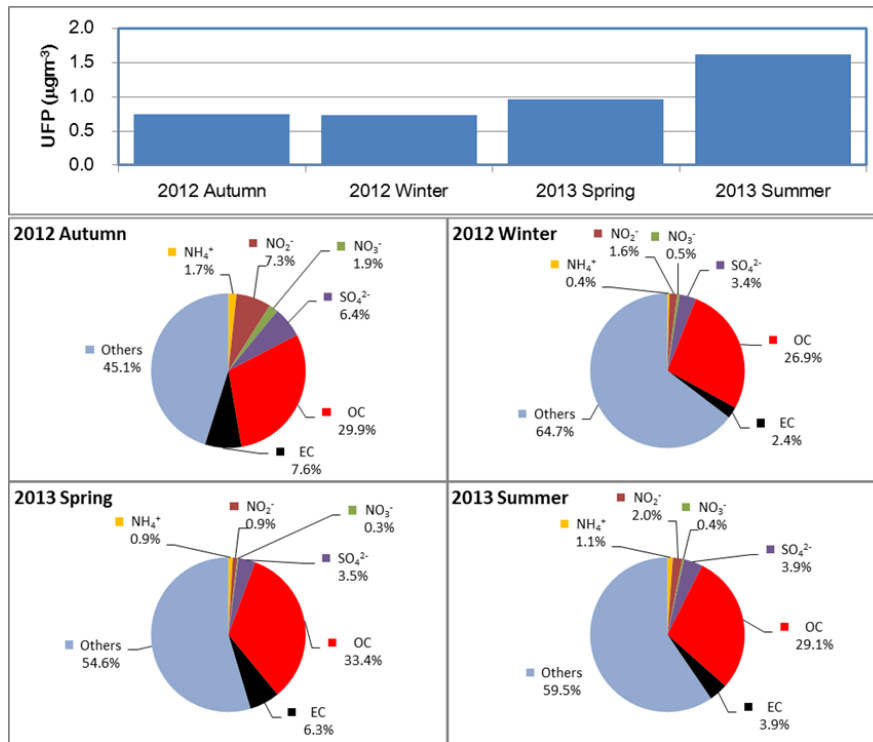
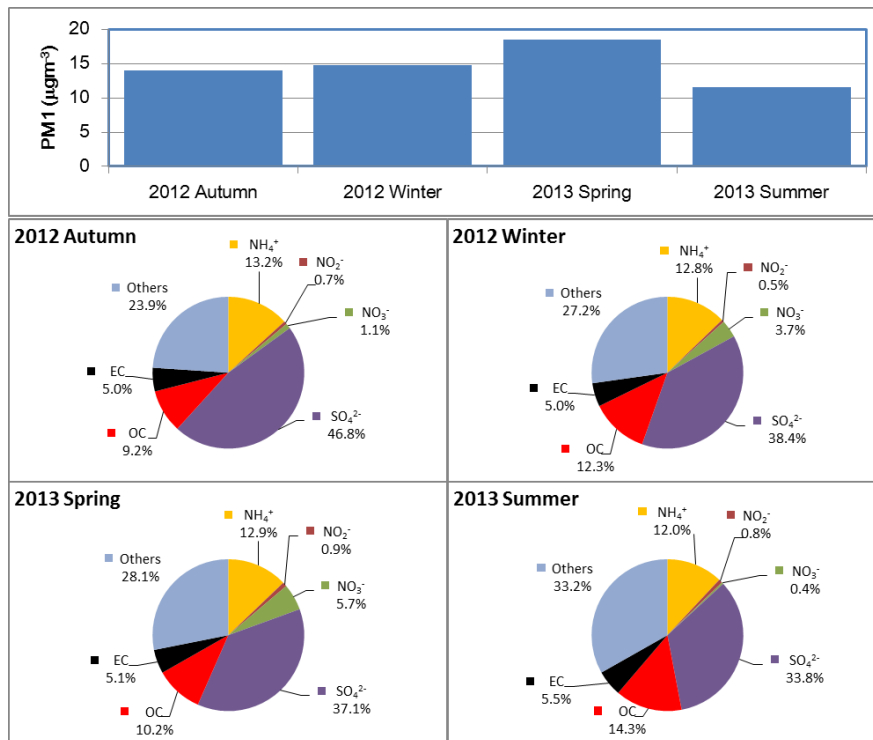


**Figure 2.** Size distribution of particle number (upper panel), surface and volume (lower panel) concentrations measured in (a) autumn, (b) winter, (c) spring and (d) summer (by curve fitting).

877  
878



879

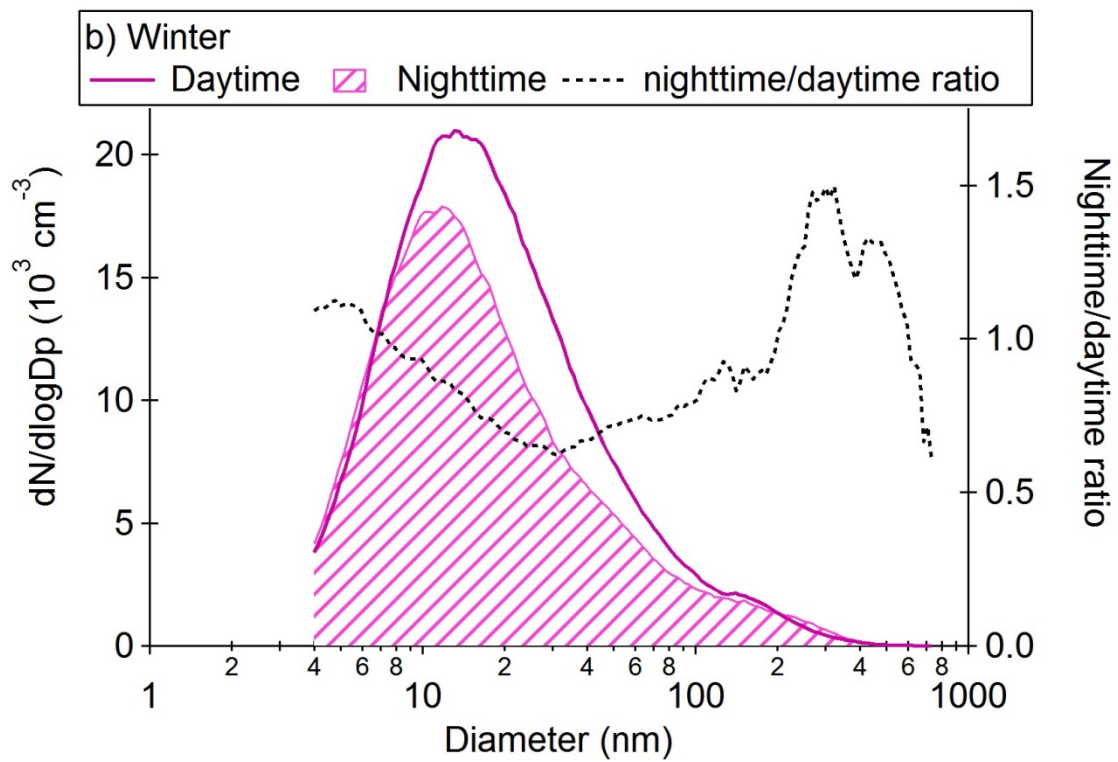
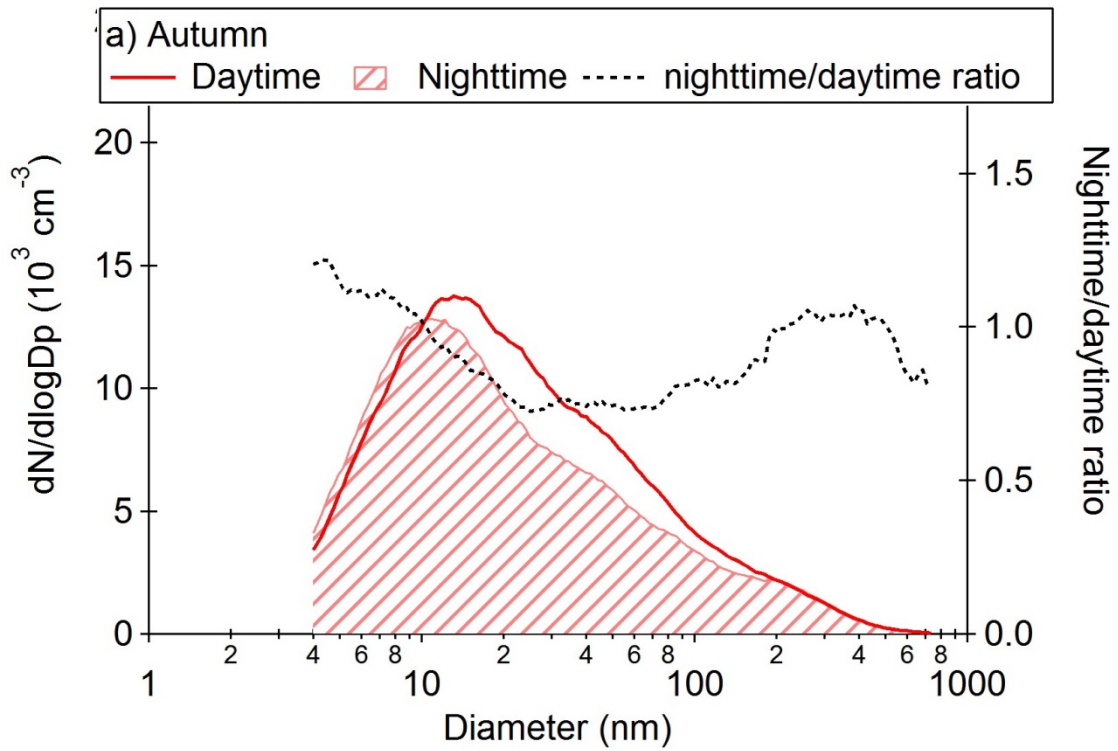


880

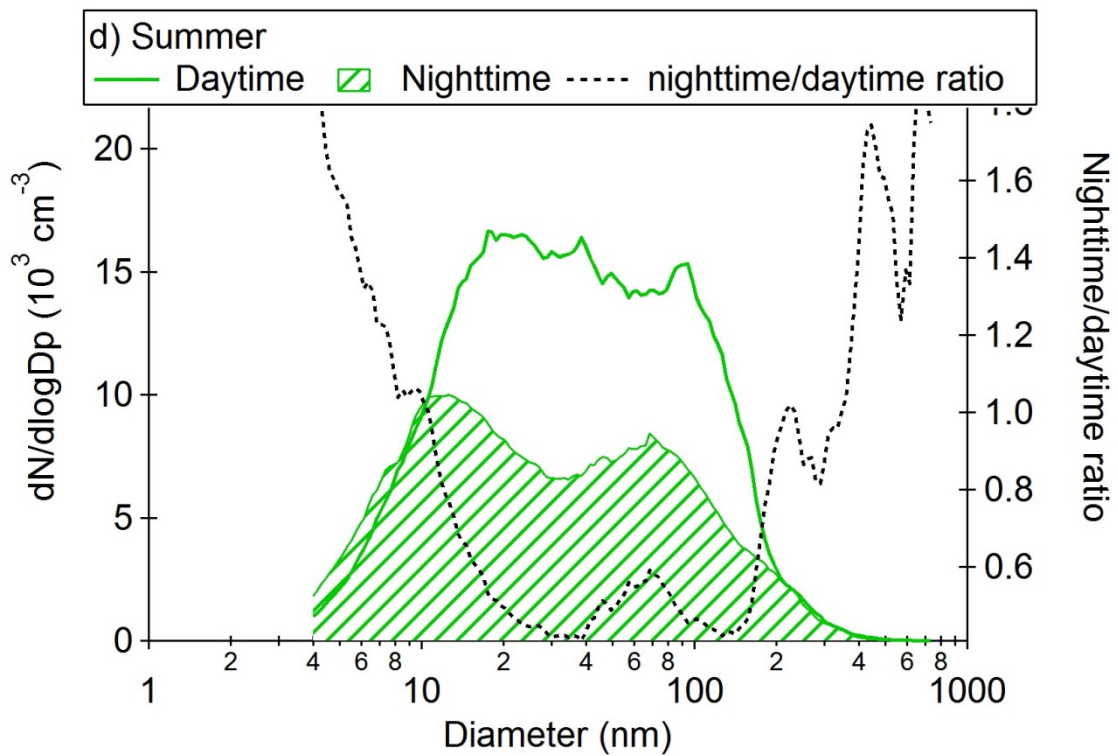
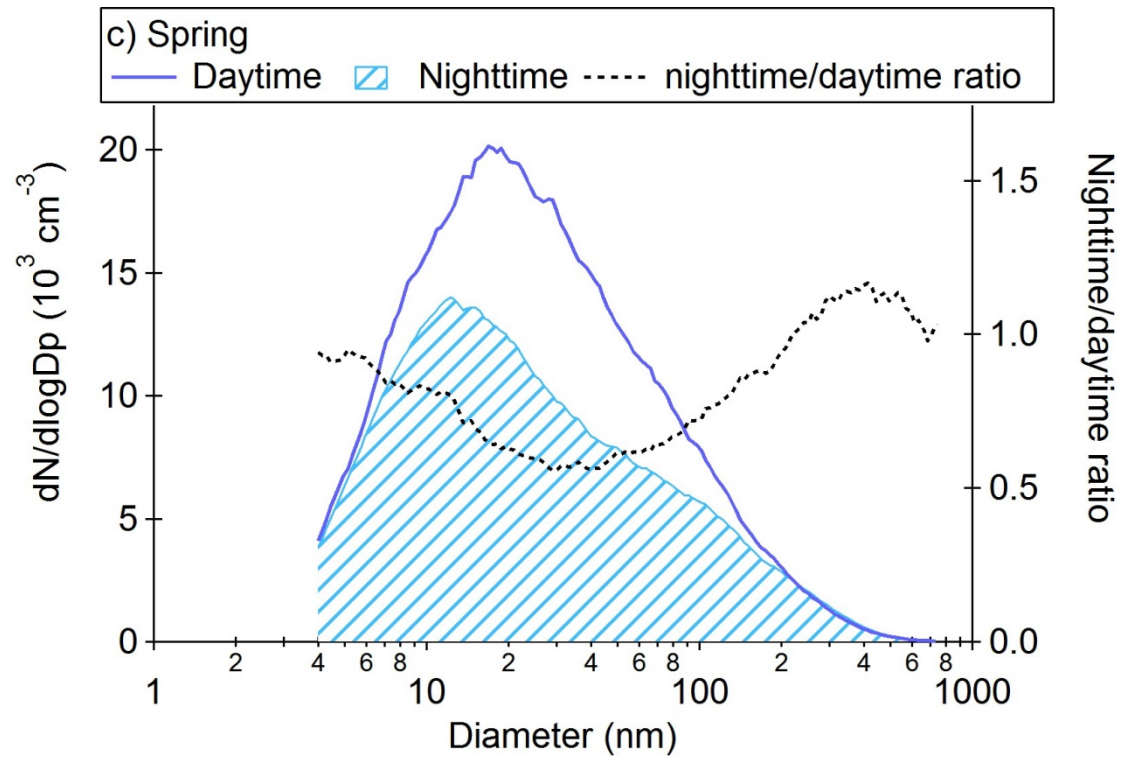
881

882 **Figure 3.** Seasonal average concentration and composition of (a) ultra-fine (UFPs) and (b)  
883 sub-micron (PM<sub>1</sub>) particles observed at the TARO in Taipei, Taiwan from autumn 2012 to  
884 summer 2013.

885

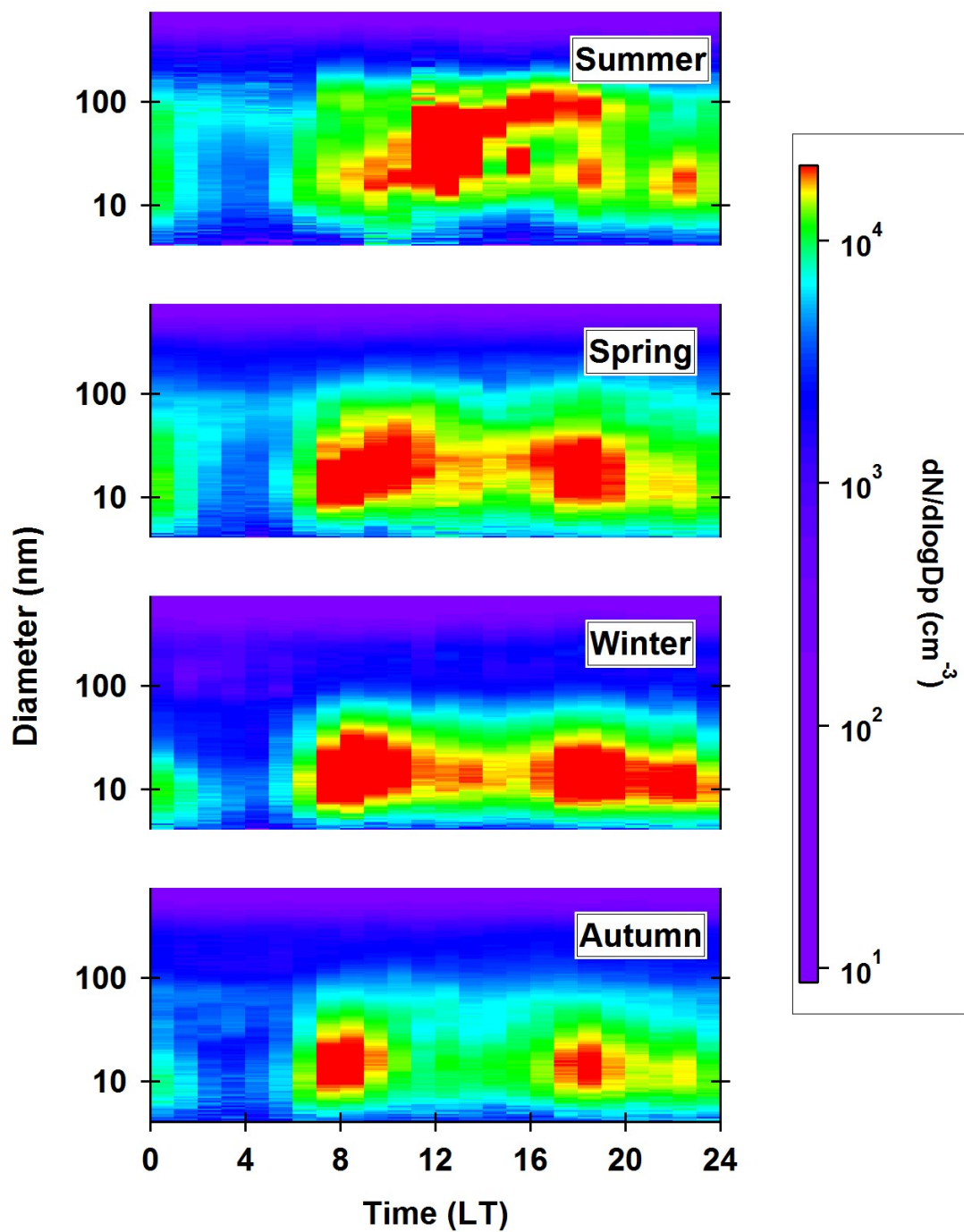


886  
887  
888  
889  
890  
891  
892  
893



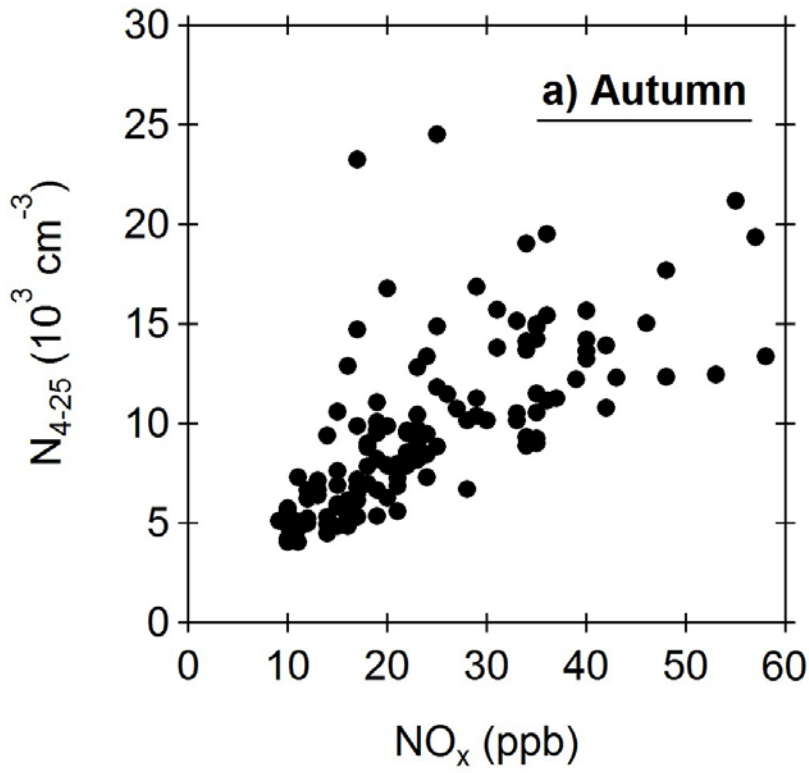
894  
895  
896  
897  
898  
899  
900

**Figure 4.** Median PSDs measured during the daytime (07:00 – 17:00 LT) and nighttime (17:00 – 07:00) in (a) autumn, (b) winter, (c) spring and (d) summer.

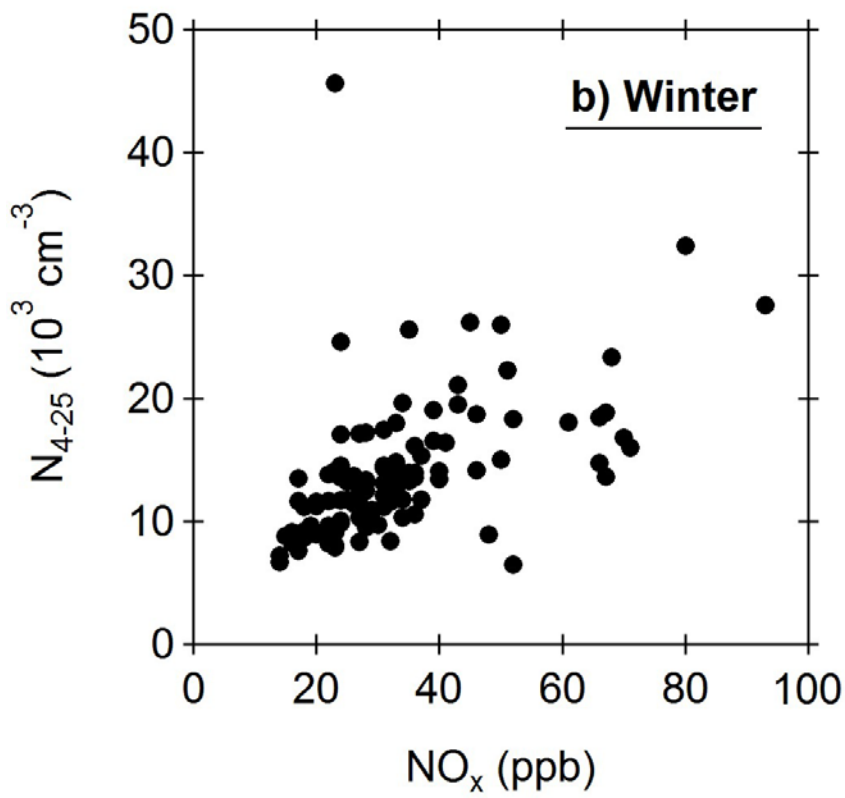


901  
 902  
 903  
 904  
 905  
 906

**Figure 5.** Diurnal variation of particle number size distribution in each season. From lower panel to top panel: autumn, winter, spring and summer.

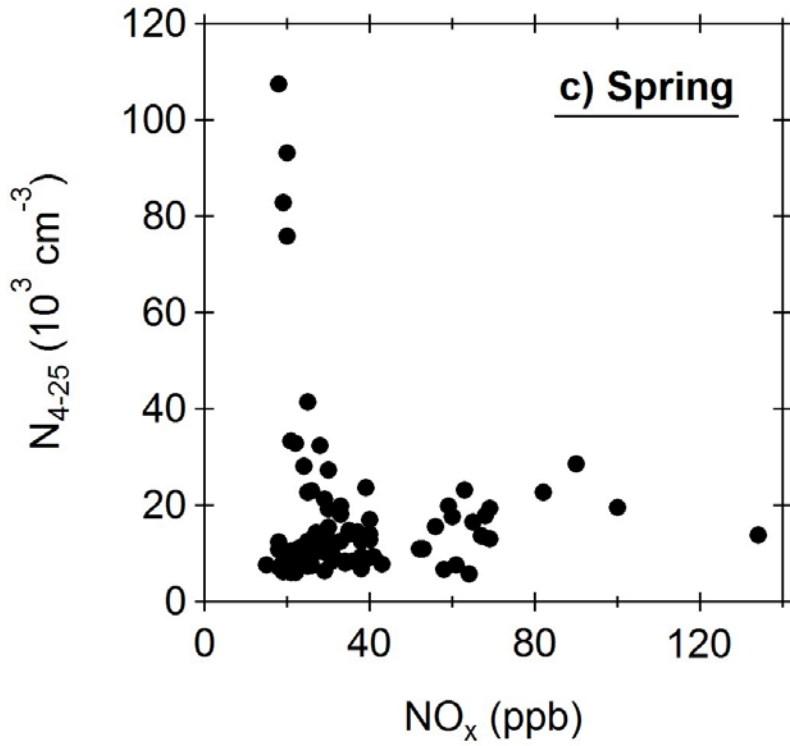


932

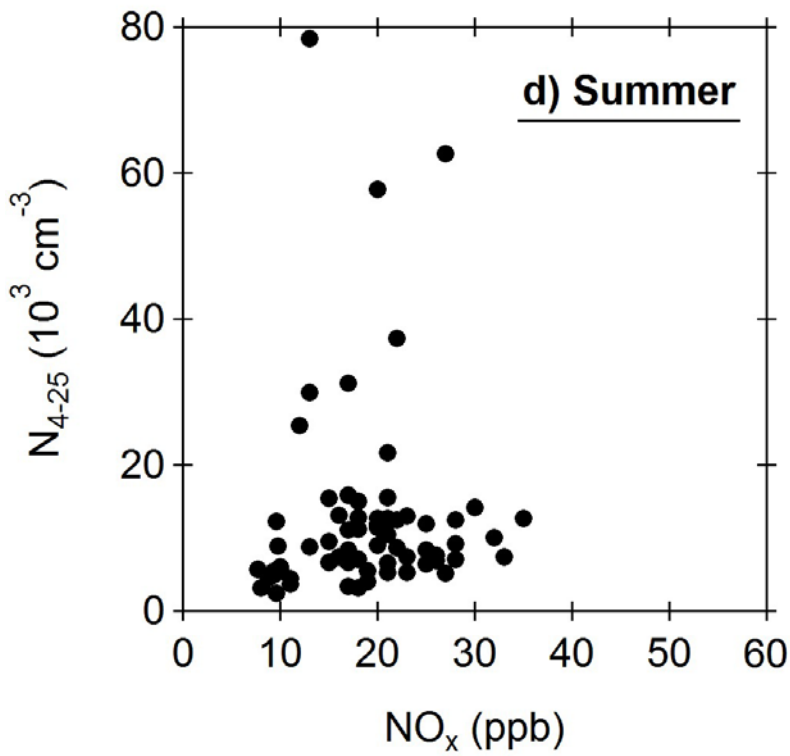


936

959  
960  
961  
962  
963



988

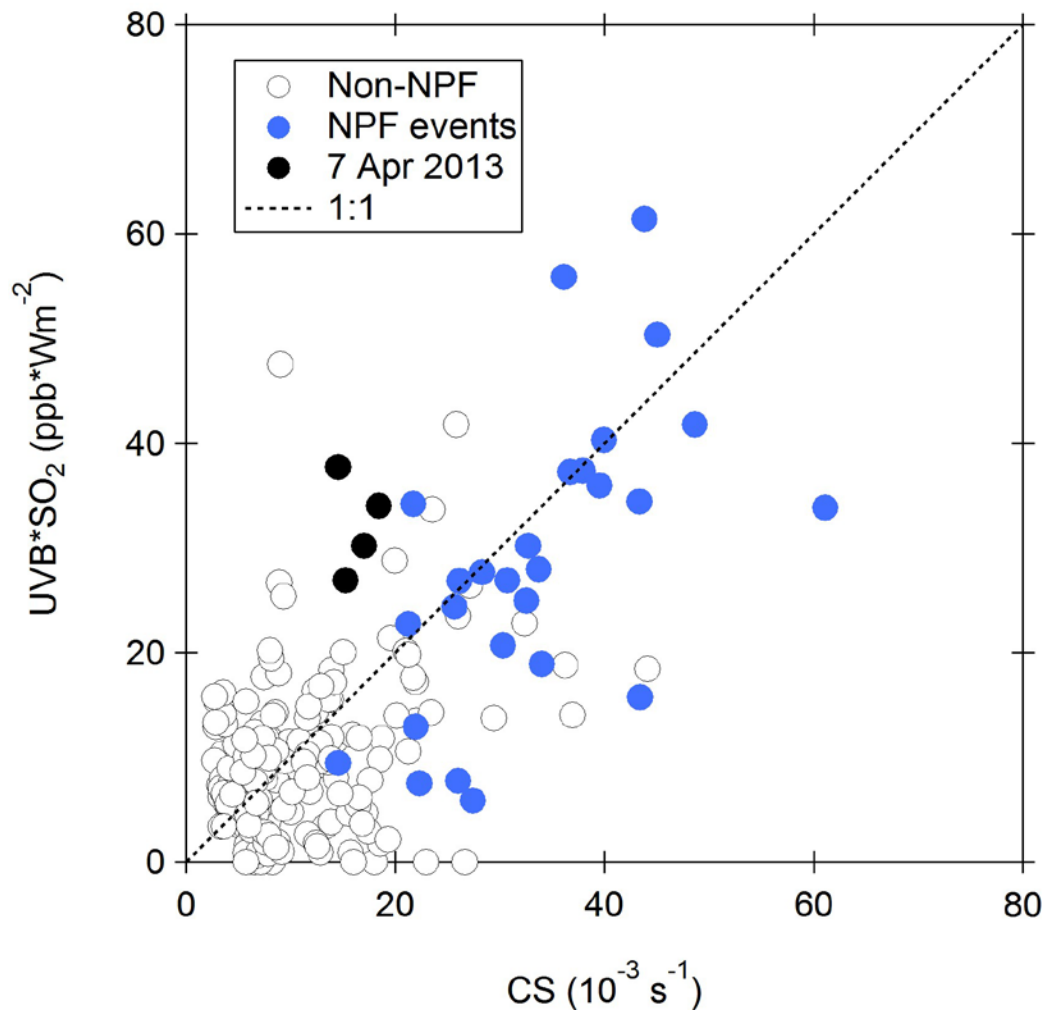


1013

1014 **Figure 6.** Scatter plots between hourly  $N_{4-25}$  and  $NO_x$  observed in (a) Autumn, (b) Winter, (c)  
 1015 Spring and (d) Summer at TARO site during the period of 07:00 – 17:00 LT.

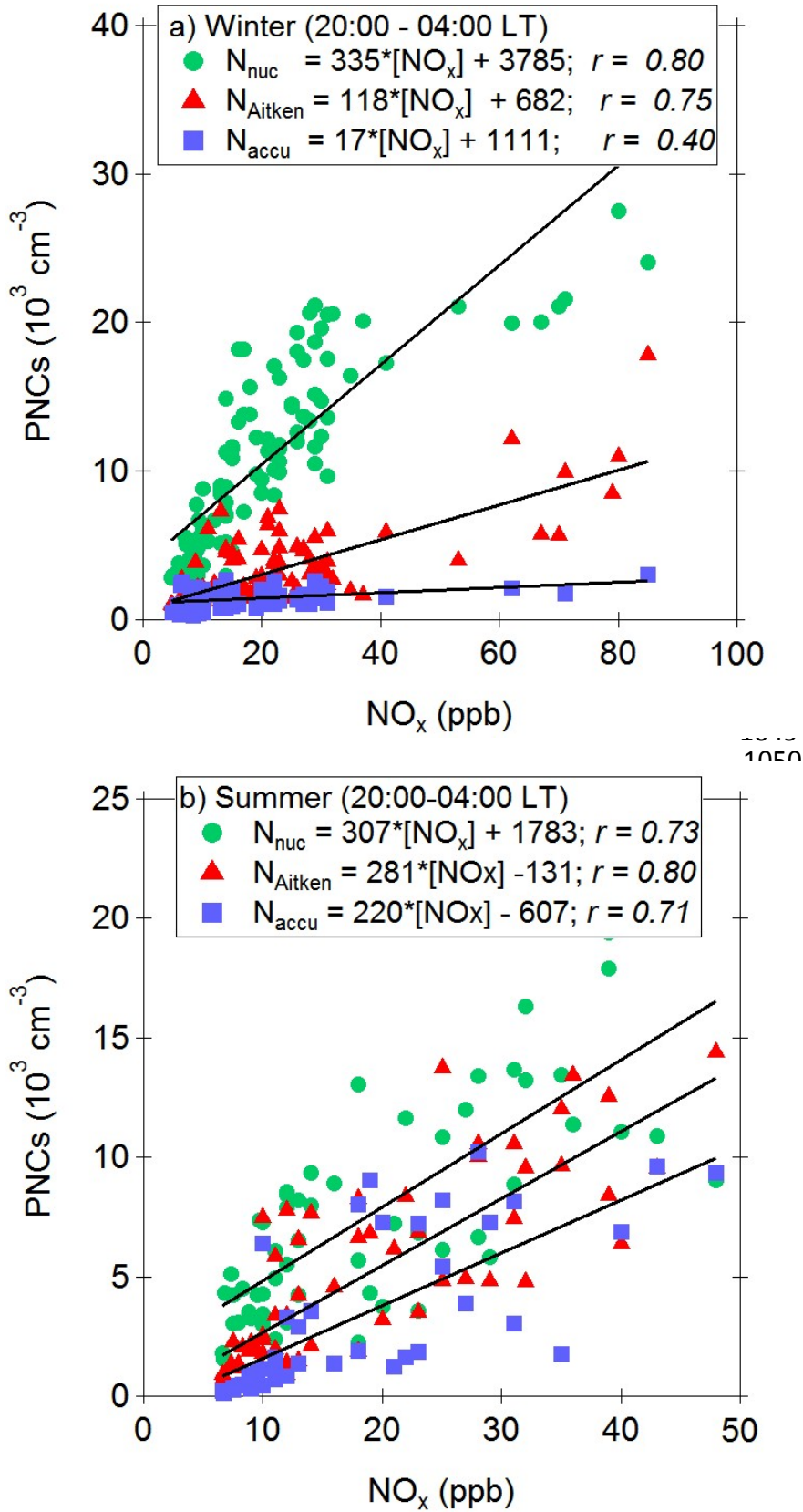
1016

1017



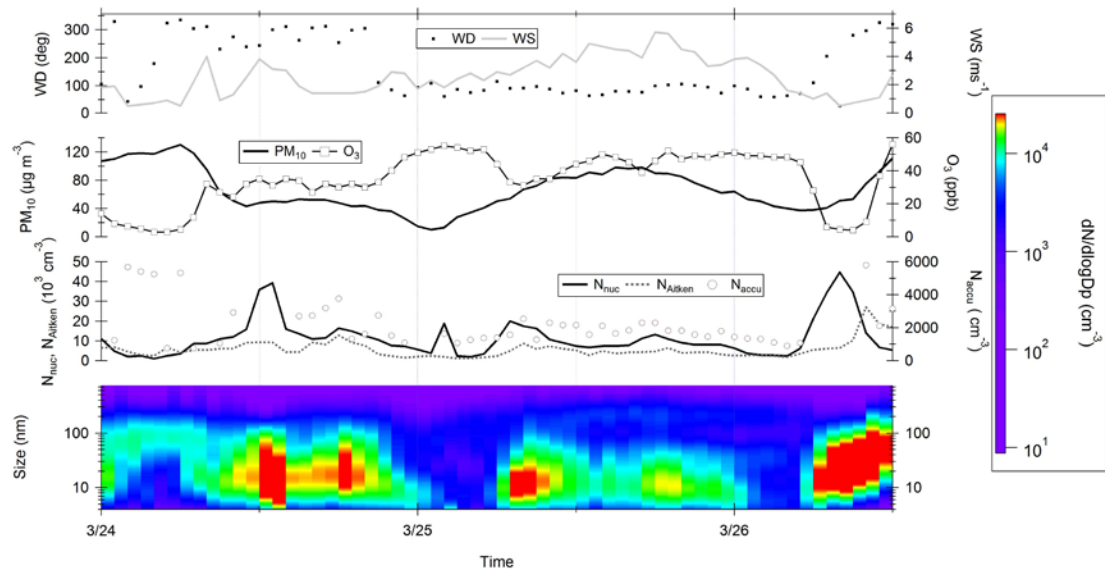
1018  
 1019  
 1020  
 1021  
 1022  
 1023

**Figure 7.** Scatter plot of hourly averaged  $UVB * SO_2$  versus condensation sink at noontime (10:00 – 14:00 LT).



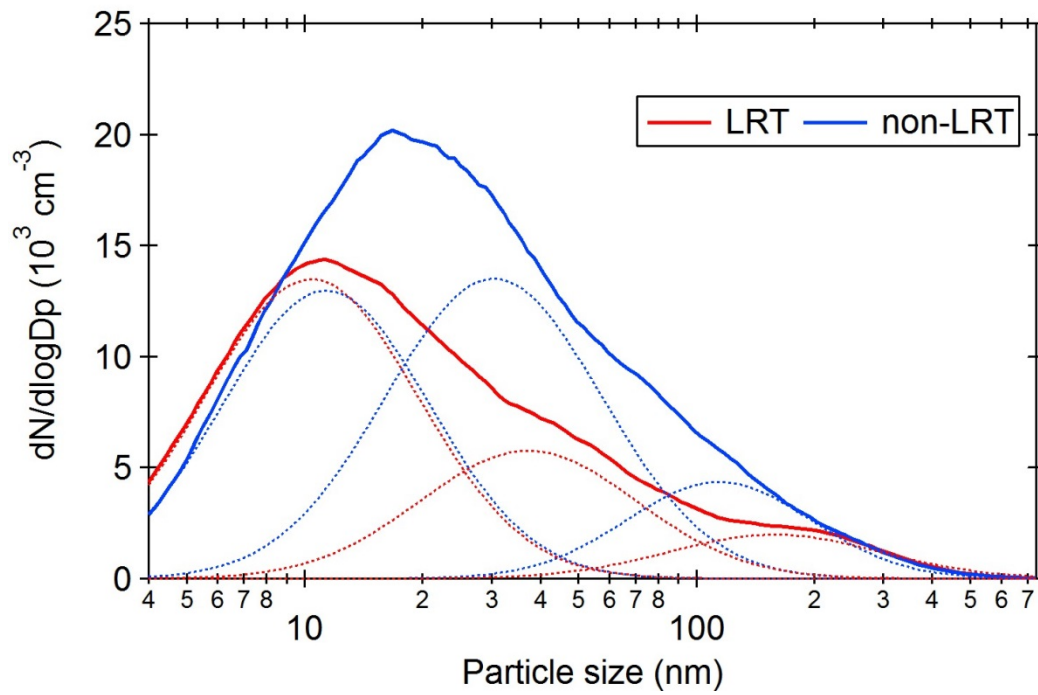
1077  
 1078  
 1079  
 1080

**Figure 8.** Scatter plots for hourly averaged PNCs vs.  $NO_x$  measured during the time period of 20:00 – 04:00 (LT) in (a) winter and (b) summer, with classification of various particle size ranges.



1081  
 1082  
 1083  
 1084  
 1085  
 1086

**Figure 9.** Time series of PSD, the  $N_{4-25}$ ,  $N_{25-100}$ ,  $N_{100-736}$ ,  $PM_{10}$ , ozone ( $O_3$ ) and wind direction/speed measured from 24 - 26 March 2013 (from bottom to top).



1087  
 1088  
 1089  
 1090

**Figure 10.** Averaged PSDs for LRT and non-LRT episodes measured during the seasons of winter monsoons. Dashed lines illustrate the PSD of each individual mode.